POLYPUBLIE
Polytechnique Montréal

POLYTECHNIQUE MONTRÉAL
UNIVERSITÉ D'INGÉNIERIE

Titre: Title:	Analysis and Implementation of the Coupled and Encapsulated Selective Frequency Damping Method
Auteur: Author:	Vincent Liguori
Date:	2021
Type:	Mémoire ou thèse / Dissertation or Thesis
Référence: Citation:	Liguori, V. (2021). Analysis and Implementation of the Coupled and Encapsulated Selective Frequency Damping Method [Mémoire de maîtrise, Polytechnique Montréal]. PolyPublie. https://publications.polymtl.ca/6281/

Document en libre accès dans PolyPublie
Open Access document in PolyPublie

URL de PolyPublie: PolyPublie URL:	https://publications.polymtl.ca/6281/
Directeurs de recherche: Advisors:	Éric Laurendeau
Programme: Program:	Génie aérospatial

Ce fichier a été téléchargé à partir de PolyPublie, le dépôt institutionnel de Polytechnique Montréal
This file has been downloaded from PolyPublie, the institutional repository of Polytechnique Montréal

https://publications.polymtl.ca

POLYTECHNIQUE MONTRÉAL
affiliée à l'Université de Montréal

Analysis and Implementation of the Coupled and Encapsulated Selective Frequency Damping Method

VINCENT LIGUORI
Département de génie mécanique

Mémoire présenté en vue de l'obtention du diplôme de *Maîtrise ès sciences appliquées*
Génie aérospatial

Avril 2021

© Vincent Liguori, 2021.

POLYTECHNIQUE MONTRÉAL
affiliée à l'Université de Montréal

Ce mémoire intitulé :

Analysis and Implementation of the Coupled and Encapsulated Selective Frequency Damping Method

présenté par **Vincent LIGUORI**
en vue de l'obtention du diplôme de *Maîtrise ès sciences appliquées*
a été dûment accepté par le jury d'examen constitué de :

Richard GOURDEAU, président
Éric LAURENDEAU, membre et directeur de recherche
Sébastien LECLAIRE, membre

ACKNOWLEDGEMENTS

This work benefited from the support of the NSERC/CRIAQ/Bombardier Aerospace Industrial Research Chair as well as from Compute Canada and Calcul Québec. We acknowledge the support of the Natural Sciences and Engineering Research Council of Canada (NSERC) towards the author through a graduate scholarship.

RÉSUMÉ

Pour répondre aux exigences de sécurité et de performances dans une enveloppe de vol de plus en plus étendue, des analyses d'aérodynamique numérique doivent être réalisées par logiciels résolvant les équations RANS sur des cas pouvant causer l'apparition de phénomènes instationnaires. Pour éviter les coûts de calculs élevés liés à la simulation de phénomène instationnaire en temps réel, une analyse sur une solution stationnaire des équations peut être effectuée. Un solveur stationnaire itératif peut cependant être incapable d'obtenir une telle solution à cause de l'instabilité liée au phénomène étudié.

L'objectif de ce projet est l'analyse et l'implémentation d'une méthode de stabilisation permettant d'obtenir une solution stationnaire quand ce problème est rencontré. Pour ce faire, la méthode "Selective Frequency Damping" (SFD) est utilisée. Deux formulations principales de cette méthode sont présentées, soit la formulation couplée et la formulation encapsulée. L'implémentation de chaque formulation est détaillée ainsi qu'une analyse mathématique simplifiée de leur effet sur une valeur propre du problème. La méthode de l'analyse de stabilité globale est également présentée comme méthode permettant d'identifier une valeur propre instable dans un écoulement. Un algorithme appelé "adaptive SFD" est finalement présenté pour stabiliser un écoulement et sélectionner les paramètres de la méthode automatiquement en utilisant la méthode de stabilité globale pour identifier un mode instable physiquement et en optimisant les paramètres en se basant sur un modèle simplifié. Des modifications sont proposées pour améliorer les méthodes existantes de la littérature, en particulier une correction périodique des variables filtrées pour accélérer la convergence du solveur et l'utilisation d'équations indépendantes du pas de temps pour optimiser les paramètres de façon à réduire le temps de calcul de cette étape.

Les deux formulations de la méthode SFD sont implémentées dans le solveur CHAMPS. La comparaison de leur stabilité révèle des limitations liées aux simplifications utilisées dans le cas d'un large pas de temps. La formulation encapsulée, l'analyse de stabilité globale et une fonction d'optimisation des paramètres sont implémentées dans le solveur NSCODE formant un algorithme "adaptive SFD". Cet algorithme est testé sur un cas de tourbillons derrière un cylindre. L'accélération de la convergence liée à la correction périodique des variables filtrées est testée. La capacité de la méthode SFD implémentée dans CHAMPS à stabiliser des écoulements sur un profil multi-éléments en condition de décrochage est démontrée.

ABSTRACT

In order to meet the safety and performance requirements in an increasingly large flight envelope, numerical aerodynamic analyses must be performed by software solving the RANS equations on cases that may cause unsteady phenomena. To avoid the high computational cost of simulating unsteady phenomena in real time, an analysis on a stationary solution of the equations can be performed. However, an iterative stationary solver may not be able to obtain such a solution because of the instability of the studied phenomenon.

The main goal of this project is the analysis and implementation of a stabilization method to obtain a stationary solution when this problem is encountered. To do this, the "Selective Frequency Damping" (SFD) method is used. Two main formulations of this method are presented, the coupled formulation and the encapsulated formulation. The implementation of each formulation is detailed along with a simplified mathematical analysis of their effect on an eigenvalue of the problem. The global stability analysis method is also presented as a method to identify an unstable eigenvalue in a flow field. An algorithm called "adaptive SFD" is finally presented to stabilize a flow field and select the parameters of the method automatically by using the global stability method to identify a physically unstable mode and by optimizing the parameters based on a simplified model. Improvements are proposed to the existing methods from the literature, in particular a periodic correction of the filtered variables to speed up the convergence of the solver and the use of equations that are not dependent on the time step to optimize the parameters in order to reduce the computational cost of this step.

Both formulations of the SFD method are implemented in the CHAMPS solver. The comparison of their stability reveals limitations related to the simplifications of the mathematical analysis when using a large time step. The encapsulated formulation, the global stability analysis and a parameter optimization function are implemented in the NSCODE solver forming an "adaptive SFD" algorithm. This algorithm is tested on a case of vortex shedding behind a cylinder. The convergence acceleration due to the periodic correction of the filtered variables is tested. The ability of the SFD method implemented in CHAMPS to stabilize cases of a multi-element profile in stall condition is demonstrated.

TABLE OF CONTENTS

LIST OF TABLES

LIST OF FIGURES

LIST OF SYMBOLS AND ACRONYMS

SFD	Selective Frequency Damping
CFD	Computational Fluid Dynamic
RANS	Reynolds Average Navier-Stokes
DNS	Direct Numerical Simulation
LES	Large Eddy Simulation
URANS	Unsteady Reynolds Average Navier-Stokes
TSM	Time Spectral Method
NLFD	Non-Linear Frequency Domain
DDES	Delayed Detached-Eddy Simulation
TADM	Temporal Approximate Deconvolution Model
ESFD	Encapsulated Selective Frequency Damping
DMD	Dynamic Mode Decomposition
GMRES	Generalized Minimal Residual
ODE	Ordinary Differential Equation
CFL	Courant-Friedrichs-Lewy

CHAPTER 1 INTRODUCTION

1.1 Context

In the domain of aircraft design and analysis, Computational Fluid Dynamic (CFD) is an indispensable tool. A numerical analysis is usually less expensive and faster than a flight test or wind tunnel testing, while the rapidly increasing computational performance available allows for numerical simulations with higher accuracy to be used earlier in the design process. Without completely replacing physical testing, numerical simulation is a tool used as an alternative and addition to greatly diminish testing and design costs.

Since the need for better aircraft efficiency has pushed design teams to explore expanded flight envelope, these tools need to be able to reliably and efficiently study flow conditions and aircraft configurations at the limit of the flight envelope. Such flight conditions can include high-lift configurations (take-off and landing) but also transonic and high-speed conditions. Unfortunately, the boundaries of the flight envelope are usually associated with unsteady phenomena that limit the use of steady CFD analysis, as shown in Fig. 1.1. In this figure, the horizontal axis corresponds to the equivalent airspeed of an airplane and the vertical axis corresponds to the loads on the aircraft structure. The combinations of these conditions for which the aircraft can fly safely are identified by an enclosed area. The limits of this area are defined by the minimum speed required to maintain sufficient lift and the speed and loading limits that would result in damage or failure of the structure.

Ensuring an accurate analysis of these conditions is particularly important from a safety standpoint because they can be associated with unsteady phenomena such as vortex-shedding and buffet. Buffet in particular can lead to flutter, a dangerous aeroelastic phenomenon in which a coupling of aerodynamic and structural forces leads to harsh vibration of the aircraft and can result in failure of the structure. This work is thus centered on providing designers with steady solutions of unsteady aerodynamic problems.

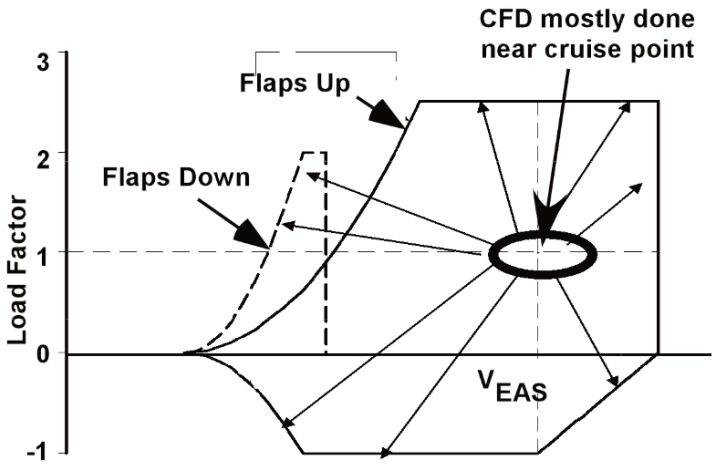

Figure 1.1 Flight envelope compared with the area for which steady CFD analysis is most reliable, reproduced from Tinoco et al. [1]

1.2 Basic concepts

1.2.1 Navier-Stokes equations

The Navier-Stokes equations are a set of partial differential equations used to describe the motion of compressible and viscous fluids. As such, they are an expression of the conservation law for mass, momentum and energy for fluids. Multiple formulations for these equations are possible, but in the context of a finite-volume CFD solver a useful formulation is the integral formulation using a convective flux vector $\vec{F_c}$ and a viscous flux vector $\vec{F_v}$ [3].

$$\frac{\partial}{\partial t}\int_\Omega \vec{W}\, d\Omega + \oint_{\partial\Omega} (\vec{F_c} - \vec{F_v})\, dS = \int_\Omega \vec{Q}\, d\Omega \tag{1.1}$$

$$\vec{W} = [\rho, \rho u, \rho v, \rho w, \rho E]^T \tag{1.2}$$

$$\vec{F_c} = [\rho V, \rho u V + n_x p, \rho v V + n_y p, \rho w V + n_z p, \rho H V]^T \tag{1.3}$$

$$\vec{F_v} = \begin{bmatrix} 0 \\ n_x\tau_{xx} + n_y\tau_{xy} + n_z\tau_{xz} \\ n_x\tau_{yx} + n_y\tau_{yy} + n_z\tau_{yz} \\ n_x\tau_{zx} + n_y\tau_{zy} + n_z\tau_{zz} \\ n_x\Theta_x + n_y\Theta_y + n_z\Theta_z \end{bmatrix} \tag{1.4}$$

where

$$\Theta_x = u\tau_{xx} + v\tau_{xy} + w\tau_{xz} + k\frac{\partial T}{\partial x} \tag{1.5}$$

$$\Theta_y = u\tau_{yx} + v\tau_{yy} + w\tau_{yz} + k\frac{\partial T}{\partial y} \tag{1.6}$$

$$\Theta_z = u\tau_{zx} + v\tau_{zy} + w\tau_{zz} + k\frac{\partial T}{\partial z} \tag{1.7}$$

$$V = n_x u + n_y v + n_z w \tag{1.8}$$

$$H = E + \frac{p}{\rho} \tag{1.9}$$

In these equations, $\vec{W}$ is the vector of conservative variables and $\vec{Q}$ is the vector of source terms corresponding to volume force and volumetric heating. In the range of aeronautics applications covered by this research, it is assumed these sources are negligible and as such they are considered equal to 0 throughout this work. Time is defined as t. The density variable is defined by ρ while the x,y and z components of the fluid velocity are respectively u, v and w. The E, H and P variable refers to the energy, the total enthalpy and the pressure of the fluid respectively. The temperature of the fluid is referred to as T. The τ_{ii} and τ_{ij} symbols refer to the viscous stresses affecting the plane perpendicular to the i-axis in the direction of the i-axis or j-axis and are represented respectively by

$$\tau_{ii} = 2\mu\left(\frac{\partial v_i}{\partial x_i} - \frac{1}{3}div(\vec{v})\right) \tag{1.10}$$

and

$$\tau_{ij} = \mu \left(\frac{\partial v_i}{\partial x_j} + \frac{\partial v_j}{\partial x_i} \right) \tag{1.11}$$

where μ is the dynamic viscosity. The thermal conductivity coefficient is referred to as k. Finally, the n_x, n_y and n_z symbols refer to normal unit vectors in their respective axis direction.

For our application it is assumed that the medium studied is a perfect gas, so the total energy E can be directly related to the pressure, density and velocity using the heat capacity ratio γ as

$$E = \frac{p}{\rho(\gamma - 1)} + \frac{u^2 + v^2 + w^2}{2}. \tag{1.12}$$

1.2.2 Reynold-Averaged Navier-Stokes equations

A popular approach to model aerodynamic flows over civil aircraft is the use of the Reynolds Average Navier-Stokes (RANS) equations. The RANS equations are based on the concept of time-averaging the original Navier-Stokes equations, which leads to the equations now solving the average value of the conservative variables. The equations solving the average variables then retain the same structure as in their original form with the exception of the addition of the Reynolds-stress tensor $-\rho\overline{v_i' v_j'}$ to the original stress tensor τ_{ij} and the addition of the so-called turbulent heat-flux vector term $-\rho\overline{h' v_i'}$ to each $k\frac{\partial T}{\partial x_i}$ term where i and j represents one of the three spatial directions, h' refers to the fluctuating static enthalpy and the v_i' notation is used to refer to a fluctuating component of a velocity [3]. These new terms create additional variables without adding equations, and as such create what is called a closure problem. This means that additional modeling for these terms is required before these equations can be solved.

1.2.3 Closure of the Reynold-Averaged Navier-Stokes equations

A popular approach, and the one used in this work, to model the additional terms related to turbulence in the RANS equations is the use of the Boussinesq's eddy viscosity hypothesis [3]. This consists in stating that the turbulent shear stress can be computed as the product of an eddy viscosity and the mean strain-rate tensor. In practice, this hypothesis can be used to simplify the additional terms related to turbulence. The Reynolds-stress tensors can be computed by adding to the laminar viscosity μ_l of the fluid a turbulent viscosity μ_t to

compute a new total viscosity $\mu = \mu_l + \mu_t$. The turbulent heat-flux vector term can similarly be computed by adding to the thermal conductivity k a turbulent thermal conductivity k_t which can be computed from the turbulent viscosity as $c_p \frac{\mu_t}{Pr_T}$ where c_p is the specific heat capacity and Pr_T is the turbulent Prandtl number, set as a constant. To solve the closure problem of the RANS equations, a model then needs to be used to compute this additional μ_t turbulent viscosity variable. Multiple models exist to do so, but in the case of this work the one-equation model of Spalart and Allmaras is used [4]. However, the theory presented could be applied to other turbulence models since the methods used are not inherently limited to this particular model.

1.2.4 Finite volume method

The use of an analytical method to solve these equations being limited to simplified problems, a discretization method is usually used. To solve the RANS equations computationally, different discretization methods can be used including finite-difference, finite-element and finite-volume. The finite-volume method is a popular method and the one used in this work. It consists in dividing the studied domain in small control volumes (so-called cells) and directly using the integral formulation of the Navier-Stokes equation on each of the cells. The fluxes are then computed on each face of the cells and summed to evaluate the residual R which is proportional to the time derivative of the flow variables. As such, when computing a steady solution the residual R is equivalent to the error of the approximate solution. The other values which are integrated in the cell volume Ω are approximated across the volume, and as such a simplified formulation of the integral Navier-Stokes equation 1.1 is used by the solver. This results in the problem written as

$$\Omega \frac{\partial \vec{W}}{\partial t} = -\overrightarrow{R}(\vec{W}) \tag{1.13}$$

where

$$\overrightarrow{R}(\vec{W}) = \oint_{\partial\Omega} (\vec{F_c} - \vec{F_v})\, dS. \tag{1.14}$$

1.2.5 Steady and unsteady solutions of the RANS equations

Another aspect that differentiates the way the equations are solved is the temporal characteristics of the solution that is expected. As seen in Eq. 1.13, a term in the equation is directly proportional to the temporal variation of the conservative variable value in the cell.

If the desired solution is steady, meaning that it has no temporal variation, this term is known to be zero for the solution. Since the steady solution is time-independent, the iterative solver can use a different time-stepping value for each cell in the domain to reach a converged solution in less computational time without a loss in accuracy. This technique is called local time stepping and is useful because the maximum time step that the solver can use is limited by stability conditions that vary across the domain, such as the cell size and the values of the conservative variables in the cell. The use of the maximum allowable time step for each cell reduces the required number of iterations to reach a steady solution but makes the transient solution physically inaccurate.

However if the desired solution is unsteady, the time evolution must be physically accurate. In this case the time step used by the solver must be consistent across all cells of the domain, otherwise referred to as global time-stepping. This requirement limits the allowable time step in almost all cells since the time step of the most limiting cell must be used. A method used to circumvent this limitation is the dual time-stepping approach. It consists in using two different time-stepping schemes to advance the problem. The first one represents the global physical time step, while the second is a local time-stepping scheme used to calculate the next physical solution. The method, as presented by Jameson [5], modifies the original equations so that a new problem can be defined where the physical temporal variation is taken into account in the residual. Consider Eq. 1.13, where the temporal scheme used to advance the flow in time globally is a second order time-accurate explicit scheme using a 3-point backward-difference approximation to calculate the derivative in time. This results in the equation

$$\frac{3}{2\Delta t}(\Omega\vec{W}^{n+1}) - \frac{4}{2\Delta t}(\Omega\vec{W}^{n}) + \frac{1}{2\Delta t}(\Omega\vec{W}^{n-1}) = -\vec{R}^{n+1} \tag{1.15}$$

where n+1 defines the current time step. This equation is then modified to be treated as a steady state problem in pseudo-time t^*, such that

$$\Omega\frac{\partial\vec{W}^*}{\partial t^*} = -\vec{R}^* \tag{1.16}$$

where $\vec{W}^*$ corresponds to the conservative variables of the current time step (n+1) and $\vec{R}^*$ is defined as

$$\vec{R}^* = \vec{R} + \frac{3}{2\Delta t}(\Omega\vec{W}^*) - \vec{Q}^* \tag{1.17}$$

$$\vec{Q^*} = \frac{4}{2\Delta t}(\Omega \vec{W}^n) - \frac{1}{2\Delta t}(\Omega \vec{W}^{n-1}). \tag{1.18}$$

The resulting equation is a steady state problem that can be solved using the same methods as the ones used when searching for steady state solutions. The solution found then corresponds to one time step of the time-accurate unsteady calculation.

1.2.6 Nondimensionalization

Comparing flow field properties from different test cases and different computational simulations can become difficult if no nondimensionalization is used. Nondimensionalization consists in multiplying or dividing a variable by characteristic physical values to remove all physical dimensions from it. This in turn allows comparing similar test cases and values that are not initially equal because their physical dimensions are different. Three nondimensional constants are particularly used throughout this work. The first one is the Reynolds number

$$Re = \frac{\rho U L}{\mu} \tag{1.19}$$

where ρ, U and μ refer to the free stream density, the free stream velocity and the free stream dynamic viscosity of the fluid respectively. L refers to a length characteristic value, in our case the chord of the airfoil or the diameter of a considered cylinder. This nondimensional constant represents the ratio of inertial forces over viscous forces within the fluid. The Mach nondimensional constant is also used, defined by

$$Ma = U/c \tag{1.20}$$

where U refers to the fluid velocity and c refers to the speed of sound. Another nondimensional constant specific to oscillating phenomena used is the Strouhal number

$$St = \frac{fL}{U} \tag{1.21}$$

where the f variable refers to the frequency of an unsteady phenomenon.

In addition to these nondimensional constants, the nondimensionalization of eigenvalues is also done in this work. The reason for this is that in the context of numerical methods used, the evolution in time of the flow is approximated as an eigenvector that is multiplied by an

exponential function written as

$$e^{\mu_o \Delta t} \tag{1.22}$$

where μ_o is the eigenvalue corresponding to the eigenvector and Δt is an interval in time. The dimensional units of μ_o in this equation are $\frac{1}{[t]}$. To compare the value of μ_o used in this work with values of similar test cases in the literature, nondimensionalization is useful. This is done by multiplying the eigenvalues μ_o by a characteristic length and dividing by a characteristic speed. Since the units of the characteristic speed are a length divided by time, this results in cancelling the time units of the original dimensional eigenvalues.

1.2.7 Unsteady phenomena

Aerodynamic unsteady phenomena can be encountered for a large variety of flow conditions and surface geometries. A well-known unsteady phenomenon is the vortex-shedding of a cylinder at low Reynolds number, the so-called von Kármán vortex street [6]. Airfoil at a low Reynolds Number can also experience the vortex-shedding phenomenon near the stall angle because of flow separation [7]. Another type of instability that is encountered in the aeronautical field is the transonic buffet phenomenon over an airfoil. Buffet is an instability that can appear at high speed in transonic flow conditions. This phenomenon is caused by a shock-boundary layer interaction and results in an oscillation of the shock position on the airfoil [8]. While the phenomena mentioned can be observed in bidimensional test cases, they can also be observed in tridimensional equivalent test cases in which a different superposed tridimensional physics and instability is sometimes observed [9].

1.2.8 System instability and equilibrium

When a steady state solution of the RANS equations is reached by a solver, the conservative variables in the flow field have reached an equilibrium. In a system, a point of equilibrium can be stable, unstable or have neutral stability. These situations are illustrated in Fig. 1.2 using the example of a marble at rest respectively at the bottom of a cavity, at the tip of a bump or on flat ground. While the marble is at a point of equilibrium in all situations since it is at rest, a perturbation of its position will have different results. In the stable case, the marble will return to the position pictured. In the unstable case, the marble will move away from the initial equilibrium point following the perturbation. In the neutral stability case, the marble will stay at its new position after a perturbation. Similarly, a steady state solution of the RANS equations, representing an equilibrium of the conservative variable solved, can

also be unstable.

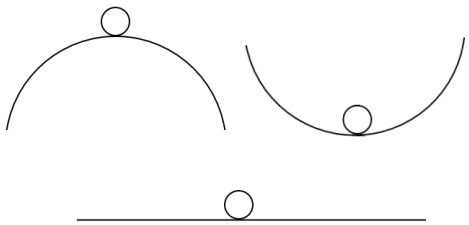

Figure 1.2 Visualization of various equilibrium points of a marble with different stability properties

A mathematical example of this stability can also be observed with a system where the evolution in time is defined by the differential equation

$$\dot{y}(t) = Cy(t) \tag{1.23}$$

where t is an independent variable and C is a constant that can be a complex number. The functions $y(t) = e^{Ct}$ and $y = 0$ are solutions of this equation. The evolution in time of these functions from an initial time t after a time step Δt is

$$y(t + \Delta t) = e^{C(t+\Delta t)} + 0 = e^{C\Delta t}(e^{Ct} + 0) = e^{C\Delta t}y(t). \tag{1.24}$$

An iterative exact solver can be used to simulate the evolution of the system in time with the operation

$$y(t + \Delta t) = e^{C\Delta t}y(t). \tag{1.25}$$

Depending on the real part of the constant C, the solution $y = 0$ can be stable or unstable when using this time-stepping operation. In the case where C has a positive real part, the solution $y = 0$ is unstable. Any initial condition that is not 0 will cause the variable to tend toward positive or negative infinity. In the case where the real part of C is equal to 0, the system will tend to oscillate according to a limit-cycle for an initial condition that is different

from 0. This also means that in both of these cases a small perturbation to the variable y from 0 will cause the solver to diverge from this value. When the C constant has a negative real part, the solution $y = 0$ is stable and the behavior of the solver is to converge toward this solution no matter the initial condition.

1.3 Elements of the problematic

The unsteady phenomena mentioned previously are problematic when encountered in the context of an analysis process for flight performance evaluation, mainly because conducting an unsteady simulation is more computationally expensive than a steady simulation by several orders of magnitude. As such, the analysis tools used can be limited in their use by the requirement of a steady-state solution. Luckily, even in conditions which result in unsteady phenomena, a steady-state solution can still exist in addition to the unsteady solution. This steady-state solution is physically unstable since the flow conditions and geometry create an unsteady phenomenon, but is still a mathematically converged solution of the RANS equations covered by the solver. Moreover, this steady-state solution can be used in the analysis process despite not being physically stable by other engineering applications and CFD analysis tools that require a steady-state solution. An example of such applications is global stability analysis, which can be used to identify and study unsteady phenomena based on converged steady-state solutions.

A problem encountered when trying to compute a physically unstable steady-state solution is that the unsteady phenomenon physic can prevent an iterative RANS solver from converging toward the desired solution by affecting the evolution of the flow. Even if the pseudo-time steps are not directly related to a time-stepping process in physical time, the unsteady phenomenon can still manifest itself in the evolving solution of this iterative process. A possible method to obtain the steady-state solution despite the unsteady physic of the phenomenon can be the use of a strong implicit solver. This approach was used by Kamenetskiy et al. [10] with a finite element solver. A similar strategy can be used by implementing a Newton solver in a finite volume solver [11, 12]. However, these methods might lack robustness for engineering applications, for instance requiring the initial solution to be inside the radius of convergence. In addition, segregated solvers might be preferred for multi-physics areas such as aero-elasticity. Hence, many flow solvers used in the industry rely on explicit Runge-Kutta schemes or Gauss-Seidel implicit schemes with an approximation of the Jacobian matrix to carry out pseudo-time iterations, for which the convergence of the solver can be prevented by an unsteady phenomenon.

Selective Frequency Damping (SFD) is a method that can be added to an iterative CFD solver to damp unsteady oscillations in the flow in time. Its concept amounts to correcting the flow computed by the solver with a filtered version of the flow that vanishes as the solver converges to a steady-state solution. This method has been studied and used in scientific literature, however its implementation in a pseudo-time stepping solver still has some challenges, particularly the selection of the parameters associated with its use. Since an unsuitable choice of these parameters can prevent a solver from converging and that they can highly vary between cases, this challenge is an important roadblock to the use of SFD in an industrial setting.

1.4 Research objectives

The main objective of this research project is to develop, implement and verify an algorithm able to damp oscillations displayed by a RANS solver that disrupt or prevent convergence so that it is able to converge to a steady-state solution of the RANS equations. The method needs to be robust and to have a limited computational cost compared with the original solver without stabilization. To respect these requirements, Selective Frequency Damping will be used inside a RANS solver. Sub-objectives are defined from this overarching main objective:

1. Compare existing formulations of SFD stabilization algorithms.
2. Investigate the potential for improvements of the existing methods.

1.5 Thesis outline

This thesis is divided in 3 main sections, which are: literature review, numerical methods and numerical results.

The literature review presents an overview of the existing knowledge concerning unsteady phenomena and their simulation, the SFD stabilization technique, the characterization and analysis of instability and the Von Neumann analysis. The numerical methods section contains a presentation of the solvers used and their particularities, a detailed mathematical presentation of the SFD formulations and the SFD parameters selection processes. It also presents the addition of a periodic reset to the SFD algorithm, the global stability analysis for the RANS equations and the adaptive SFD algorithm. The numerical results section presents the various tests on different configurations used to validate the methods, including global

stability analysis, the adaptive SFD algorithm and the optimization of the parameters. It finally addresses the stabilization of a case on a complex geometry. The document concludes on the various scientific observations and provides future research perspectives.

CHAPTER 2 LITERATURE REVIEW

2.1 Unsteady phenomena

This section presents a review of information currently available in the literature that is relevant to this work. A review of various available experimental and numerical available results for unsteady phenomena is presented. Previous developments and use in numerical experiments of the SFD method are then reviewed. The section concludes with existing methods of instability identification.

2.1.1 Vortex shedding over cylinder

The vortex shedding mechanism over bluff body has been extensively studied by the scientific community. It is a self-excited phenomenon where the separation of the boundary layer causes an unsteady oscillation in the flow resulting in the periodic shedding of vortices in the wake of the object. The so-called Karman vortex street in the wake of a cylinder is a well-known example of this phenomenon. A compilation of experiments and numerical simulation of this case has led Zdravkovich [13] to use a classification of the different flow regimes depending on the Reynolds number of the flow. The transition between a steady and unsteady phenomenon in a laminar flow is observed to be occurring at a Reynolds number of 48 and the transition between the unsteady laminar flow and an unsteady turbulent flow occurs at a Reynolds number of 180. Williamson [14] presents a continuous relationship between the Strouhal number of the instability and the Reynolds number of the flow obtained experimentally. The Strouhal number increases as the Reynolds number increases, starting at a value of 0.12 for a Reynolds number of 50. It should be noted that these values refer to a developed instability, which is different from the onset of the instability.

Numerical analysis results are available for an array of computational methods. Rajani et al. [6] presented results of URANS simulations of both bidimensional and tridimensional circular cylinders in laminar flow for various Reynolds numbers. The unsteadiness associated with the vortex shedding phenomenon is observed and the results, including the computed Strouhal number, are compared with experiments. Similar results on a bidimensional case with a Reynolds number of 180 are presented by Gopinath & Jameson [15] using a Time Spectral Method (TSM) method and by Mosahebi & Nadarajah [16] using a Non-Linear Frequency Domain (NLFD) method.

2.1.2 Buffet over transonic airfoil

The transonic regime is comprised of flows with freestream Mach numbers below 1.0, but that can locally reach speeds above the speed of sound. To revert to subsonic speed, the flow can exhibit a shock. The transonic buffet phenomenon on airfoil occurs because of an interaction between a sonic shock and the turbulent boundary layer of the airfoil. The oscillation exhibited is an oscillation of the position of the shock on the upper surface of the airfoil, accompanied by a separation of the boundary layer behind the shock when it is closer to the leading edge in its movement. It should be noted that unlike the phenomenon of vortex shedding over a cylinder, this instability requires a turbulent flow to develop. This phenomenon can eventually cause flutter on an aircraft when considering the coupling of the aerodynamical and structural models [8].

Experimental results of this phenomenon are presented by Jacquin et al. [17]. The experiment is performed in a wind tunnel with efforts to make the results close to a bidimensional case by limiting the wall effects on the results. The studied airfoil is the OAT15A, a supercritical profile. The unsteady phenomenon is observed and measured, making for useful reference values, in particular the frequency of the shock oscillation.

Grossi et al. [18] have done numerical computations of a test case similar to the experiment of Jacquin et al. [17]. The URANS and Delayed Detached-Eddy Simulation (DDES) simulation methods are used. While differences in the flow behavior are observed between the two methods, the unsteadiness frequency prediction is in agreement with the experimental results. The results also show a sensitivity to the choice of turbulence model.

Computational (RANS) testing has also been done on the OAT15A test case by Sartor et al. [19]. URANS is used to simulate the unsteady phenomenon, which is observed with good agreement with experimental results of Jacquin et al. [17]. Global stability analysis is used to characterize the onset of the unstable phenomenon. In particular, the Strouhal number and amplification factor of the unstable eigenvalue computed from global stability analysis are provided.

2.1.3 Instability of airfoil in post-stall conditions

The post-stall regime of an airfoil, which is the range of angle of attacks after its maximum lift coefficient has been reached, has been observed both experimentally [20] [21] and numerically [22] [23] to present hysteresis of steady flow solutions. This hysteresis is observed

to be associated with the separation and reattachment of the flow to the airfoil occurring at different angles of attack depending on the initial condition used [11]. The study of this behavior is made difficult by the fact that instabilities are usually encountered in these conditions. SFD is a method that has been used by Richez et al. [22] to compute these steady solutions despite their instability on the case of the single element airfoil OA209.

2.2 Selective Frequency Damping

2.2.1 Original formulation

Selective Frequency Damping [24] is a mathematical method that can be added to an existing solver with the goal of damping oscillations displayed by the solver. The method is based on the assumption that it is applied on a system that has a steady-state solution toward which it can converge, but that also exhibits an unsteady mode which prevents the complete system from converging to its steady solution. The method was first presented by Akervik et al. [24] in its original coupled formulation. This formulation adds a source term to the right-hand side of the Navier-Stokes equation to stabilize the equations. An additional equation is also added to calculate a low-pass time-filtered version of the flow, augmenting the system of equation. The method can be related to a similar source term implemented in a Large Eddy Simulation (LES) method for the Temporal Approximate Deconvolution Model (TADM) model by Pruett et al. [25].

The equation used to calculate the filtered flow is a causal temporal filter in its differential formulation, which allows for the filtering to proceed simultaneously with the evolution of the flow by the solver and limits the memory requirements of the filter implementation. The use of this filter on the Navier-Stokes equation was presented by Pruett et al. [26]. The resulting system of equation 2.1, where W refers to the physical flow variables, $\bar{W}$ refers to the time-filtered corresponding variables and $\dot{W}$,$\dot{\bar{W}}$ refers to their respective variation in time, can then be solved by an iterative solver.

$$\begin{cases} \dot{W} = f(W) - \chi(W - \bar{W}) \\ \dot{\bar{W}} = \frac{W - \bar{W}}{\Delta} \end{cases} \tag{2.1}$$

Two main points are stressed. The first one is that the method adds two parameters to the equations. The first one is the χ parameter, which scales the magnitude of the additional source term. It is called the control coefficient. The second parameter is the Δ parameter, which corresponds to the cutoff wavelength of the low-pass time filter. These parameters

need to be set by the user to suitable values. The suitable range of values varies between different instabilities. The second main point is that while the method allows the solver to reach a steady state solution that it could not have reached otherwise, the method itself does not create any additional solutions since the source term vanishes when a steady state is reached.

The equations and their developments are presented with more details in the numerical methods section of this document, however a description of the analysis of the method provided by Akervik [24] is relevant to this section. Multiple possibilities could have been selected for the second equation corresponding to the calculation of the causal low-pass time filter, corresponding to other filter kernels. The used filter is selected for its simplicity. The effect of the modification of the equation is studied through an analysis of the modification of the eigenvalues of the linearized equation system. It is observed that while SFD is able to make unstable eigenvalues of a high enough frequency more stable, the inverse effect can be observed for eigenvalues of a low enough frequency. However, another observation is that no eigenvalue that is already stable can be made unstable because of SFD. Based on this analysis and practical observations, an approximate methodology is proposed to manually get a rough estimate of suitable parameter values. In a related analysis, Passaggia & Ehrenstein [27] presented a development relating the eigenvalues of the modified system with stabilization to the eigenvalues of the original system.

Akervik et al. [24] present successful results of stabilization with an implementation of this technique for a Direct Numerical Simulation (DNS) method on the case of a bidimensional flow over a long cavity. The method with this formulation is used by numerous authors for simulations of a variety of cases including the case of jet in a crossflow [28] [29], the case of a lifted flame [30] [31], the case of the wake of a sphere [32] and thin aerofoil wake [33]. More recently Moise [34] successfully used SFD to obtain a steady solution of a bubble vortex breakdown in a laminar swirling jet.

It should be noted that it was reported by Jones & Sandberg [35] that an attempt was made to stabilize the case of tonal airfoil self-noise over the NACA0012 airfoil using SFD. However, the authors were not able to obtain a flow corresponding to a steady state solution of the Navier-Stokes equation by using SFD despite trying multiple values for the χ and Δ parameters and allowing long time integration. The authors hypothesized that the reason for this failure to apply the method was that a very large damping parameter χ is needed to damp the oscillations observed for this case, which results in an impractically long time-integration

requirement to converge. This highlights the importance of the choice of parameters on the performance of the method, and the fact that its application has limits that can depend on the implementation, the accuracy of the method used to select the parameters and the instability being studied.

2.2.2 Alternative formulations

Following this original formulation, an important improvement to the method was presented by Jordi et al. [36] with the Encapsulated Selective Frequency Damping (ESFD). ESFD is an alternative formulation for the implementation of SFD. The rationale for the development of this new formulation is that the original formulation of SFD requires significant modifications to an existing CFD solver, with the calculation of an additional source term and solving an augmented set of equations. A way to avoid this difficulty is proposed with a new implementation where the original solver is segregated from the solving of the calculation of the low-pass time filtered flow and the correction of the flow by the source term.

This segregation of the equations in two steps is based on a mathematical method named sequential operator-splitting [37]. This method is based on the hypothesis that using time steps to advance multiple differential equations representing different physical phenomena iteratively in time using the solution of the preceding one as the initial condition of the subsequent will result in a good approximation of advancing in time an equation where all the different physics are taken into account. The possibility to solve multiple smaller equations makes the solving of multi-physics problems significantly easier. ESFD takes advantage of this benefit by allowing the original Navier-Stokes equation problem to be solved by the original solver with no modification and the subsequent problem being solved by a direct solver requiring very minimal computing power. A possible downside of sequential operator splitting however is that the segregated advancement in time of the different equations results in a loss of temporal accuracy.

The ESFD formulation was used by various authors since its presentation. This includes Casacuberta et al. [38] which used it successfully to stabilize the case of vortex shedding from a cylinder using DNS. A case of tridimensional buffet over a wing using a RANS method was stabilized by Plante et al. [23]. Other cases were also stabilized by various authors such as the case of shear driven cavity flow by Bengana et al. [39], natural circulation system by Pini et al. [40] and laminar separation bubble by Rodriguez et al. [41].

Implementations with alternative development were also presented recently in the literature. Plante & Laurendeau [42] presented an implementation based on ESFD with a local selection of the Δ parameter value with the goal of damping numerical oscillations and as such increase the convergence rate of a steady-state solver using the RANS equations. Paladini et al. [43] presented another alternative where the stabilizing source term of SFD is applied on selected regions of the solved domain only, with the goal of identifying which region could be stabilized to prevent the appearance of the unsteady phenomena. Numerical results are presented for the case of transonic buffet over an airfoil using URANS.

2.2.3 Parameters selection

Because of the importance of parameter selection on the behavior of the solver regarding convergence, multiple authors proposed methodologies to set these parameters. Akervik et al. [24] presented a heuristic methodology approximating suitable values based on preliminary knowledge of the eigenvalue related to the unstable mode. It is mentioned that this methodology should only be considered as a general guideline.

Jordi et al. [44] presented such a method, which they called adaptive SFD. The idea behind this method is to periodically run a global stability analysis on a partially converged flow and use the dominant unstable eigenvalue found to estimate the characteristics of the instability to damp. An optimization is then run to optimize the selection of the χ and Δ parameters to maximize the damping of this eigenvalue.

Cunha et al. [45] present a similar method using Dynamic Mode Decomposition (DMD) to identify the dominant eigenvalues. A notable difference and addition when compared to the previous algorithm is that in this case the algorithm considers other eigenvalues in addition to the dominant unstable one in the optimization by setting a minimum damping for all eigenvalues identified.

Casacuberta et al. [38] present a methodology based on observing the development of the instability in relation to the time iteration to estimate the dominant eigenvalue defining the instability and the one limiting the convergence rate. They then present a developed mathematical analysis of the effect of parameter choice on both unstable and stable eigenvalues. Their method is notable for optimizing the value of the χ and Δ directly by solving an equation that uses both the unstable eigenvalue and the stable but convergence limiting eigenvalue, but requires manual observation of the convergence rate or an automatic

convergence rate detection functionality.

Plante & Laurendeau [42] set a local value for the Δ parameter based on the objective of accelerating the rate of convergence of the solver with good results. However this parameter selection is not based on the objective of stabilizing an unsteady phenomenon preventing a solver from converging, instead assuming the frequency of the numerical oscillations to be damped based on knowledge of the underlying equations.

2.3 Instability identification

Many methods are available to identify and characterize instabilities in time-dependent flows of numerical simulations. Oscillation detection is a research subject in itself and more complete reviews of the different methods are available [46]. Some notable methods used in the literature for detection and characterization of instabilities in the field of CFD simulations with the aim of stabilization by SFD are presented in this section.

A method that can be used in the absence of a better alternative is a visual observation of the unstable flow. This simple method is mentioned by Akervik et al. [24] for an estimation of suitable parameters. This method has many drawbacks and limitations. For instance, the characterization is limited to the evaluation of the frequency of the instability. In addition, this method is subjective, prone to noise and not automated. Richez et al. [22] similarly used probes in different regions of the flow to determine the lowest frequency to damp.

A method used by Cunha et al. [45] is Dynamic Mode Decomposition. This method is based on estimating the eigenvalues of the jacobian matrix defining the evolution of the flow by correlating the evolution of the flow with a matrix multiplication and identifying the eigenvalue of the matrix defining this evolution. Numerical results have shown the method is able to identify eigenvalues of the flow with good accuracy.

However a limitation of methods based on analysis of limit-cycle oscillations is that the evolution of the unstabilized flow in these oscillations may differ from the dynamic of the linearly growing unsteady mode because of the non-linearity of the equations. This means that the eigenvalues of the flow's jacobian matrix obtained from a limit-cycle oscillation may differ from the eigenvalues of the stabilized flow's jacobian matrix when the studied case has a non-critical Reynolds number [47].

Global stability analysis is a method that can be used in CFD to analyze unstable aerodynamic phenomena. Jordi et al. [44] notably use this method to obtain the unstable eigenvalue related to vortex shedding over a cylinder. It is based on the idea of studying the linearized equations of the system around a solution point. The Jacobian matrix of the linearized equation is then computed by finite difference so that its eigenvalues can be evaluated [48]. Crouch et al. [2] used global stability analysis to predict the offset of flow unsteadiness on the cases of laminar flow around a cylinder and transonic flow around an airfoil. The results show good agreement with experiments and unsteady simulations.

An important benefit of this method is that since it is based on a linearization of the equation around a flow field, the eigenvalues obtained represent the behavior of the instability during its linear rising phase instead of its limit-cycle oscillation behavior. This would be a disadvantage if the goal was to describe the developed instability, but in this case where the goal is to characterize the instability when it appears this is actually a wanted feature. A limitation of this method is that the computational cost of the matrix eigenvalue solving is high and scales with the size of the mesh, limiting the use of the method for larger meshes that would result in larger global matrices. Another limitation of the method is that to facilitate the calculation of the eigenvalues of interest in the matrix, an initial estimation of the eigenvalues is needed. This is somewhat alleviated by the fact that general relationships and previous experiments can help a user to roughly estimate the eigenvalues related to the unstable phenomenon.

Casacuberta et al. [38] use a method specifically designed to be used in conjunction with SFD, which they call SFD unleashed. Their methodology is to conduct a SFD run using a pair of parameters χ and Δ manually selected without optimization to get a partial convergence on the test case. Once this is achieved, SFD is turned off and a perturbation noise is applied to the flow field. This triggers the appearance of the unstable mode and allows the observation of the linear growing phase of the mode. The frequency of the mode is evaluated through the use of probes in the field. The growth rate of the mode is evaluated by measuring the upward slope of the norm of the residual of the low-pass time filter equation, which can be fitted with an exponential function in the linear growth regime. The eigenvalue limiting the convergence is then evaluated by measuring with the same method the downward slope of the same residual when SFD is applied.

This method has the benefit of obtaining the values of relevant eigenvalues in the linear growth phase which is of interest for stabilization. However, it is based on observation of the

flow evolution and as such requires either manual observation or a dedicated analysis functionality that can handle different cases since the linear growth phase needs to be identified.

CHAPTER 3 NUMERICAL METHODS

This section presents the numerical algorithm used in this work. First, a description of the solvers used and their capabilities is provided. The mathematical definition of the stabilization method, SFD, its implementations and an analysis of its effects are then shown. Finally, the instability identification method used, the global stability analysis, is detailed and the complete algorithm used to damp an unsteady oscillation is presented.

3.1 CFD solvers

Two distinct CFD solvers, "NSCODE" and "CHAMPS", are used in this project. Both of them solve the RANS equations with a finite-volume method. However, they differ in some of their capabilities and the programming language in which they are coded. The most important difference between them is that NSCODE requires 2D structured meshes while CHAMPS works on 2D and 3D cases and unstructured meshes.

3.1.1 NSCODE

NSCODE is a CFD software developed by professor Éric Laurendeau's team at Polytechnique Montréal [49]. It is coded in C with shared-memory local thread parallelization using OpenMP and is linked to a Python interface to allow for more modularity when using different functionalities.

This software solves the RANS or URANS equations using a cell-centered finite-volume approach. The convective fluxes are computed by a central scheme [50] with either scalar or matrix artificial dissipation [51]. The required mesh type for the solver is a 2D structured grid. Convergence can be accelerated with a multi-grid functionality and residual smoothing.

The solver solves steady and unsteady simulations. In the case of steady simulations, local time-stepping is used and two temporal schemes are available, namely the explicit hybrid five-stage Runge-Kutta scheme and the implicit Lower-Upper Symmetric-Gauss-Seidel scheme. Multiple turbulence models are implemented in the solver such as the Baldwin-Lomax algebraic model [52], the Spalart-Allmaras model with compressibility correction and Edwards-Chandra modification [4] [53] [54] and the Menter $k-\omega$ SST model [55].

Other available functionalities include an overset grid functionality and frequency-domain solver for time periodic problems. The $\gamma - Re\theta_t$ model [56] is also implemented and can be used conjointly with the $k-\omega$ SST model for laminar to turbulent flow transition prediction.

3.1.2 CHAMPS

CHAMPS, which stands for Chapel Multiphysics Simulation, is the latest CFD software developed by professor Éric Laurendeau's team at Polytechnique Montréal [57]. It is coded using the Chapel language. The software supports shared memory and distributed memory parallelism through the use of native functionalities of the Chapel language.

In a similar manner to NSCODE, CHAMPS solves the RANS or URANS equations using a cell-centered finite-volume approach. The convective fluxes are computed using the Roe scheme [58]. The flow variables gradients used to achieve second-order spatial accuracy can be computed with the Green-Gauss or Weighted Least Square methods. Gradient limiters implemented include the Barth-Jespersen and the Venkatakrishnan limiters. The mesh type used by CHAMPS is either 2D unstructured or 3D unstructured. The solver includes a residual smoothing functionality for convergence acceleration, however unlike NSCODE no multi-grid functionality is available in this solver.

The solving of both steady and unsteady simulations is possible. In the case of steady simulations, local time-stepping is used. Multiple temporal schemes are implemented, including the explicit hybrid five-stage Runge-Kutta scheme and the implicit Lower-Upper Symmetric-Gauss-Seidel and Generalized Minimal Residual (GMRES) schemes. Available turbulence models include the Spalart-Allmaras model and the $k-\omega$ SST model. A more detailed description of the CHAMPS software and its performance was presented by Parenteau et al. [57].

3.2 Selective frequency damping implementation

In this section, the Selective Frequency Damping method is detailed mathematically. This includes a presentation of the different formulations implemented and their stabilization effect. The parameter selection methodology is then detailed. Finally, the new addition to the algorithm of a periodic reset is presented. It should be noted that the implementation of SFD in this work uses a "frozen turbulent viscosity" approach, which means that the stabilized variables are the density, velocity components and pressure. The turbulent viscosity variable

coming from the turbulence model is not directly stabilized and is solved by a segregated iterative solver in the software used. For this reason, the mathematical developments presented in this section do not consider the turbulent viscosity variable.

3.2.1 Coupled Selective frequency damping

The coupled formulation of SFD is the first one that was presented by Akervik et al. [24]. This formulation is implemented in the CHAMPS software. As presented in section 1.2.4, Eq. 1.13 defines the original equations solved by a CFD solver. For simplicity, this original equation can be written as a general differential equation, where the dot notation ($\dot{W}$) is used to indicate a time-derivative. The vector notation is omitted for simplicity since the SFD equations introduce no interactions between the different variables in a system of equations. The equations can then be demonstrated for a scalar with no loss of generality regarding an application to matrix equations. This results in

$$\dot{W} = f(W) \tag{3.1}$$

in which $f(W)$ denotes the residual R, equivalent to the summation of the convective fluxes, viscous fluxes and source terms (if any) divided by the cell volume. A steady-state solution W_s is sought so that $f(W_s) = 0$. To allow the solver to converge to the steady state in the presence of unsteady oscillations, a source term proportional to the difference between the variable and the steady-state solution can be added to the original equation:

$$\dot{W} = f(W) - \chi(W - W_s). \tag{3.2}$$

This additional source term is tantamount to a proportional controller, a well-known concept in control theory, with the χ parameter being equivalent to a proportional gain. When the steady state is reached, the additional source term will amount to zero since in this case $W = W_s$. As such, a solution of this new system of equations is also a solution of the original equation.

In practice the steady state is not known in advance, if it was the solver would not be necessary. To counter this limitation, a low-pass time-filtered version of the flow, represented as $\bar{W}$, is used in place of the actual steady-state value:

$$\dot{W} = f(W) - \chi(W - \bar{W}). \tag{3.3}$$

The idea behind the use of a low-pass filter is that the filtered version of the unconverged flow, while not necessarily a solution of the RANS equations, will have significantly damped oscillations compared to the solver. As such the coupling of this filtered flow with the physical flow will still be able to drive the flow solver toward a steady solution. Since a steady state has no temporal variation, as the solver gets closer to a steady state the low-pass time-filtered version of the flow will also approach a steady state, until the low-pass time-filtered version of the flow and the flow itself both have converged to a steady state. By ensuring that both the physical flow and the low-pass time-filtered flow have the same values, it can then be confirmed that the steady solution obtained is a solution of the original equations.

The use of a low-pass time-filtered version of the physical flow requires the calculation of this filtered flow. Hence, a new equation must be defined to implement a low-pass time filter for the flow field. Since the filtering is done as the calculation progresses, a causal filter is necessary. Multiple filters could be used for this task, but the one selected is the one used by Akervik et al. [24]. This filter is a first order low-pass time filter, which in integral formulation can be written:

$$\bar{W}(t) = \int_{-\infty}^{t} \frac{1}{\Delta} exp(\frac{\tau - t}{\Delta}) W(\tau) d\tau. \tag{3.4}$$

The integral formulation is not very practical to implement the filter since the integration in time requires the storage of all previous values of the filtered flow [24]. This would lead to potentially limiting memory requirements. The equivalent differential formulation

$$\dot{\bar{W}} = \frac{W - \bar{W}}{\Delta} \tag{3.5}$$

is preferred for this reason. The original system of equations is then augmented with the additional filter equation for each variable to simultaneously solve for the low-pass time-filtered value of the flow.

The complete augmented set of differential equations for the coupled SFD method is defined by this matrix equation, where W, $\bar{W}$, $\dot{W}$ and $\dot{\bar{W}}$ are column vectors containing all conservative variables of the cells of a considered mesh:

$$\begin{bmatrix} \dot{W} \\ \dot{\bar{W}} \end{bmatrix} = \begin{bmatrix} f(W) \\ 0 \end{bmatrix} + \begin{bmatrix} -\chi I & \chi I \\ \frac{1}{\Delta} I & \frac{-1}{\Delta} I \end{bmatrix} \begin{bmatrix} W \\ \bar{W} \end{bmatrix}. \tag{3.6}$$

The implementation of this formulation in an existing CFD software requires multiple modifications to the solver. To illustrate this fact, an explanation of how this formulation modifies the linear system of equation considered by the solver is provided below.

The spatially-discretized matrix equations solved by a finite-volume RANS CFD solver are presented in Eq.1.13. These equations must also be discretized in time to obtain a linear system of equations that can be solved numerically. The temporal scheme used to numerically advance these equations from a flow field W_n at time t_n to a flow field W_{n+1} at time t_{n+1} can be based only on values already known at time t_n to compute the residual R_n, in which case it is considered that an explicit temporal scheme is used. The equation with this type of scheme can be written as

$$\Omega(\Delta t)^{-1}\Delta W = -R_n \tag{3.7}$$

where

$$\begin{aligned} \Delta W &= W_{n+1} - W_n \\ \Delta t &= t_{n+1} - t_n. \end{aligned} \tag{3.8}$$

It should be noted that, since these equations represent the calculation of the whole flow field, the variable used represent matrices. The size of these matrices is defined by the number of degrees of freedom, which is the number of cells in the field that will be considered equal to m and the number of variables solved. For a laminar 3D case, 5 variables are solved corresponding to density, velocities in the x,y and z directions and pressure. The Ω matrix then consists of the diagonal matrix

$$\begin{bmatrix} \Omega_1 & & 0 \\ & \ddots & \\ 0 & & \Omega_m \end{bmatrix} \tag{3.9}$$

where each Ω_i element is actually a 5x5 diagonal matrix where each diagonal element is equal to the volume of the i^{th} cell in the field. The Δt matrix is defined similarly, with the difference that the diagonal elements are equal to the time step used for the i^{th} cell. The ΔW and R variables correspond to column vectors of size mx1 of which each element is actually a 5x1 column vector containing respectively the flow variables mentioned earlier and the residuals

corresponding to the sum of the fluxes for each of these variables. For example, the R matrix is defined with the column vectors

$$\begin{bmatrix} R_1 \\ \vdots \\ R_m \end{bmatrix} \tag{3.10}$$

where an element R_i can be written as

$$R_i = \begin{bmatrix} R_{i\,\rho} \\ R_{i\,\rho u} \\ R_{i\,\rho v} \\ R_{i\,\rho w} \\ R_{i\,\rho E} \end{bmatrix}. \tag{3.11}$$

The detailed formulas of the elements of these R_i column vectors can be found in the book of Blazek [3]. A notable difference between this matrix equation and the general equation used to present SFD in Eq. 3.1 is the Ω term present on the left-hand side, which is not present in Eq. 3.1. This term could theoretically be brought to the right-hand side to better match the original generic equation, but is actually kept in the left-hand side in the assembled system used by the solvers of this project. To compensate for the fact that this term is present outside of the residual, the additional terms introduced by SFD will be multiplied by this term so that it can cancel itself during the linear solving of the system and correspond to the original formulation.

From this simple explicit temporal scheme, we can define the more complex implicit temporal scheme, which uses the residual at the next time step

$$\Omega(\Delta t)^{-1}\Delta W = -R_{n+1}. \tag{3.12}$$

To approximate this residual, a linear approximation is done using the Jacobian matrix

$$\frac{\partial R}{\partial W} = \begin{bmatrix} \frac{\partial R_1}{\partial W_1} & \cdots & \frac{\partial R_1}{\partial W_m} \\ \vdots & \ddots & \vdots \\ \frac{\partial R_m}{\partial W_1} & \cdots & \frac{\partial R_m}{\partial W_m} \end{bmatrix} \tag{3.13}$$

in which each element $\frac{\partial R_i}{\partial W_j}$ corresponds to a 5x5 matrix where the derivative of each residual

is calculated for each conservative variables. An approximation of the complete residual equation is usually used for the calculation of this matrix [3]. In practice, the majority of the $\frac{\partial R_i}{\partial W_j}$ matrices are null matrices, since the fluxes calculated at the faces of a cell are only influenced by a limited amount of neighboring cells. However, the diagonal elements $\frac{\partial R_i}{\partial W_i}$ are not null matrices since they represent the influence of the value of the variables inside a cell on the fluxes calculated at its own faces. The residual at the next time step R_{n+1} is then defined based on the current residual, the current conservative variables of the flow and the variables being calculated for the next time step

$$R_{n+1} = R_n + \frac{\partial R_n}{\partial W} \Delta W \tag{3.14}$$

resulting in the new system

$$\left(\Omega (\Delta t)^{-1} + \frac{\partial R_n}{\partial W} \right) \Delta W = -R_n. \tag{3.15}$$

With this definition of the original matrix system, we can then observe the modifications applied to it by the addition of SFD, starting with the explicit temporal scheme. The new augmented SFD system is comprised of matrices with the same structure of matrix elements as the one presented previously for the original system. The difference lies in the definition of the smaller element matrices that they contain. In the case of the explicit temporal scheme, the SFD augmented system consists in

$$\Omega_{SFD} (\Delta t_{SFD})^{-1} \Delta W_{SFD} = -R_{SFD,n}. \tag{3.16}$$

The ΔW_{SFD} matrix is once again composed of a certain number m of matrix elements, corresponding to the m cells in the domains. The matrix elements in question are now 10x1 column vectors that can be written as

$$\Delta W_{SFD\ i} = \begin{bmatrix} \Delta W_i \\ \Delta \bar{W}_i \end{bmatrix} \tag{3.17}$$

for the i^{th} element, where the ΔW_i matrix is identical to the original matrix 5x1 columns vectors mentioned in the presentation of the original system. The $\Delta \bar{W}_i$ is also a 5x1 column vector, containing the equivalent filtered variables. The Ω_{SFD} and Δt_{SFD} matrices are once again block-diagonal matrices of size mxm, with the smaller i^{th} matrices on the diagonal $\Omega_{SFD\ i}$ and $\Delta t_{SFD\ i}$ being 10x10 matrices containing the volume and time step of the cell on

their diagonal elements.

A particular attention is provided to the R_{SFD} matrix since the modifications in its case are more extensive. This matrix is also once again a mx1 block-matrix, with each element being a 10x1 column vector. An i^{th} element can be written in function of the original 5x1 R_i elements presented in Eq. 3.11 as

$$\begin{bmatrix} R_{i,n} - \chi\Omega_i(W_{i,n} - \bar{W}_{i,n}) \\ \bar{R}_{i,n} \end{bmatrix} \tag{3.18}$$

where the 5x1 $\bar{R}_i$ column vector can be detailed as

$$\bar{R}_{i,n} = \frac{1}{\Delta}\Omega_i(W_{i,n} - \bar{W}_{i,n}). \tag{3.19}$$

The appearance of the Ω_i matrix in the terms added by SFD is necessary to compensate for the multiplication of the left-hand side of the equation by the Ω matrix, as mentioned earlier.

In the case of the implicit time-stepping scheme with the addition of SFD, the matrix system consists of

$$\left(\Omega_{SFD}(\Delta t_{SFD})^{-1} + \frac{\partial R_{SFD,n}}{\partial W_{SFD}}\right)\Delta W_{SFD} = -R_{SFD,n}. \tag{3.20}$$

The matrices in this system are the same as the ones presented above, with the addition of the $\frac{\partial R_{SFD}}{\partial W_{SFD}}$ matrix. This matrix once again has a similar structure as the original $\frac{\partial R}{\partial W}$ matrix, being defined as

$$\frac{\partial R_{SFD}}{\partial W_{SFD}} = \begin{bmatrix} \frac{\partial R_{SFD,1}}{\partial W_{SFD,1}} & \cdots & \frac{\partial R_{SFD,1}}{\partial W_{SFD,m}} \\ \vdots & \ddots & \vdots \\ \frac{\partial R_{SFD,m}}{\partial W_{SFD,1}} & \cdots & \frac{\partial R_{SFD,m}}{\partial W_{SFD,m}} \end{bmatrix} \tag{3.21}$$

in which each element $\frac{\partial R_{SFD,i}}{\partial W_{SFD,j}}$ corresponds to a 10x10 matrix where the derivative of each residual is calculated for each conservative variable of the original equations and their filtered counterpart. Since the original residual vector is still present in the augmented residual vector and the terms added with SFD only relate each variable with its corresponding counterpart, the additions to the complete matrix are limited to three diagonals. This results in:

$$\frac{\partial R_{SFD,i}}{\partial W_{SFD,j}} = \begin{bmatrix} \frac{\partial R_i}{\partial W_j} & 0I_{5\text{x}5} \\ 0I_{5\text{x}5} & 0I_{5\text{x}5} \end{bmatrix} + \begin{bmatrix} -\chi\Omega_j I_{5\text{x}5} & \chi\Omega_j I_{5\text{x}5} \\ \frac{1}{\Delta}\Omega_j I_{5\text{x}5} & \frac{-1}{\Delta}\Omega_j I_{5\text{x}5} \end{bmatrix} \tag{3.22}$$

where $I_{5\text{x}5}$ is used to denote an identity matrix of dimensions 5x5 and $0I_{5\text{x}5}$ is used to denote this same matrix multiplied by 0, which results in an empty 5x5 matrix. Finally, Ω_j denotes once again a diagonal 5x5 matrix with the volume of the j^{th} cell on its diagonal.

These modifications must also be considered from a programming perspective. To store the values of the conservative variables of the filtered flow, new memory must be allocated. The size required is the same as the one used by the base flow conservative variables. Regarding the solver, since the system of equation is augmented, the memory allocated for the matrices of the solver must also be increased for the low-pass filter equation, Eq. 3.5. A function must be added to compute the proportional feedback source term of Eq. 3.3 and add it to the sum of the fluxes during a solver iteration. A function must also be added to compute the right-hand side of the filter equation. Depending on the architecture of the code for the solver, more extensive modifications may be needed to apply the temporal scheme and to solve the new filter equations.

A CFD solver is usually a complex program, and as such these modifications can be hard to implement in an existing solver without compromising its performances. For this reason, the coupled formulation presented in this subsection is not implemented in the NSCODE software. This formulation is implemented in the CHAMPS software since the architecture of the software is particularly well suited for the augmentation of the system of equations that the coupled SFD requires.

3.2.2 Encapsulated Selective frequency damping

An alternative implementation of SFD was proposed by Jordi et al. [36] with the goal of reducing the modification needed to an existing solver to apply SFD. The so-called Encapsulated Selective Frequency Damping is based on the operator-splitting method. This method consists in segregating a system of Ordinary Differential Equation (ODE) in multiple simpler sub-problems. This method is particularly useful in multiphysics problems, where the various physical models used can have different accuracy and stability requirements for the length of the time steps resulting in impractically high computational cost. The functionality of operator-splitting can be demonstrated with a generic Cauchy problem where we assume that A and B are linear operators in the form of matrices and W is a column vector of the

variables that need to be solved

$$\begin{aligned} \frac{\partial W}{\partial t} &= AW + BW \\ t \ \in \ [0,T],\ W(0) &= W_0. \end{aligned} \tag{3.23}$$

With a defined time interval of $t_{n+1} - t_n = \Delta t$, the exact solution of the problem in the time interval is

$$W_{n+1} = e^{\Delta t(A+B)} W_n. \tag{3.24}$$

If for any reasons already mentioned this equation is impractical to solve in its original form by an iterative solver, operator-splitting aims to segregate the original problem into two simpler sub-problems:

$$\begin{aligned} \frac{\partial W}{\partial t} &= AW \\ t \ \in \ [0,T],\ W(0) &= W_0, \end{aligned} \tag{3.25}$$

$$\begin{aligned} \frac{\partial W}{\partial t} &= BW \\ t \ \in \ [0,T],\ W(0) &= W_0. \end{aligned} \tag{3.26}$$

Each sub-problem can then be solved by an iterative solver, potentially a different one for each problem, with the best time step value for each problem. The result of each sub-problem over the same time interval are then

$$W_{n+1} = e^{\Delta t A} W_n \tag{3.27}$$

and

$$W_{n+1} = e^{\Delta t B} W_n. \tag{3.28}$$

The two sub-problems should of course still be linked, and multiple algorithms exist to make the two sub-problems interact in an approximation of the original problem. The goal of course is that this approximation of the original problem results in a solution of sufficient accuracy compared with a solution of the original problem.

The particular splitting method used in this case is sequential operator-splitting with the Lie-Trotter algorithm [37]. Using the analytical solution of each problem to calculate a progression in time, which represents the effect of an exact solver, the algorithm in the case of the current example of Eq. 3.23 results in the following steps.

First, the first sub-problem (Eq. 3.25) is advanced in time by a defined time step to get a temporary solution

$$W_{n+0.5} = e^{\Delta tA} W_n. \tag{3.29}$$

This temporary solution is then used as the initial condition of the other sub-problem (Eq. 3.26, which is advanced in time subsequently by the same time step

$$W_{n+1} = e^{\Delta tB} W_{n+0.5}. \tag{3.30}$$

The result of the iteration of the algorithm, which will be used as the initial condition of the first sub-problem in the next iteration, is then

$$W_{n+1} = e^{\Delta tB} e^{\Delta tA} W_n. \tag{3.31}$$

When comparing this solution with the solution of the original problem, shown in Eq. 3.24, one can see that the two equations are equal if the A and B matrix operators are commutative. If this is not the case, an error exists between the evolution in time of the operator-splitting solution and the original solution. This error means that the use of operator-splitting introduces a loss of time-accuracy when compared to solving the original problem. The sequential operator-splitting shown above has been demonstrated in the literature to have a local splitting error of second order and as such is a first order scheme [37].

While the SFD matrix equation of Eq. 3.6 is not originally a linear differential equation, its linearized formulation using the jacobian matrix of the original RANS equations is one.

This makes the previous analysis relevant to the SFD equations, both to demonstrate how sequential operator-splitting is able to approximate the original solution and the loss of time-accuracy. To apply this sequential operator-splitting algorithm to the SFD equations, the terms from the original equation which will define the sub-problems must be identified. The fluxes and source terms of the original RANS equations are used to define the first sub-problem, while the proportional feedback source term and the calculation of the low-pass filtered flow are used to define the second sub-problem.

The first sub-problem then consists of

$$\begin{cases} \dot{W} = f(W) \\ \dot{\bar{W}} = 0 \end{cases} \tag{3.32}$$

which is the initial RANS equation problem. The original RANS solver is already able to solve this problem iteratively, and as such the first subproblem is advanced in time with

$$\begin{bmatrix} W_{n+0.5} \\ \bar{W}_{n+0.5} \end{bmatrix} = \begin{bmatrix} \Phi(W_n) \\ \bar{W}_n \end{bmatrix} \tag{3.33}$$

where $\Phi(W)$ represents the action of the solver over one iteration.

The second sub-problem consists of

$$\begin{cases} \dot{W} = -\chi(W - \bar{W}) \\ \dot{\bar{W}} = \frac{W - \bar{W}}{\Delta} \end{cases}, \tag{3.34}$$

which are the terms added to apply the SFD method. This problem is in fact a linear differential equation

$$\begin{bmatrix} \dot{W} \\ \dot{\bar{W}} \end{bmatrix} = L \begin{bmatrix} W \\ \bar{W} \end{bmatrix} = \begin{bmatrix} -\chi I & \chi I \\ \frac{1}{\Delta} I & \frac{-1}{\Delta} I \end{bmatrix} \begin{bmatrix} W \\ \bar{W} \end{bmatrix}. \tag{3.35}$$

This linear differential equation can be easily solved analytically, and as such the second sub-problem can be iterated in time with an exact solver consisting in a simple matrix multiplication

$$\begin{bmatrix} W_{n+1} \\ \bar{W}_{n+1} \end{bmatrix} = e^{L\Delta t} \begin{bmatrix} W_{n+0.5} \\ \bar{W}_{n+0.5} \end{bmatrix} \tag{3.36}$$

where the $e^{L\Delta t}$ operator is

$$e^{L\Delta t} = \frac{1}{1+\chi\Delta}\begin{bmatrix} I + \chi\Delta I e^{-(\chi+\frac{1}{\Delta})\Delta t} & \chi\Delta I(I - Ie^{-(\chi+\frac{1}{\Delta})\Delta t}) \\ I - Ie^{-(\chi+\frac{1}{\Delta})\Delta t} & \chi\Delta I + Ie^{-(\chi+\frac{1}{\Delta})\Delta t} \end{bmatrix}. \tag{3.37}$$

The iterative solving of the two sub-problems of ESFD is very simple provided that an iterative solver for the original equation already exists since the solver can be used on the original problem and the second sub-problem can be advanced in time with a simple matrix product. To implement this formulation, memory must be allocated for the filtered variables, a function must be added to compute the matrix product to advance the second sub-problem in time and a function must be added to compute the added residual of the low-pass filter function. No resizing of the matrices of the original solver is necessary. These modifications are much less extensive than for the original coupled SFD. For this reason, this encapsulated formulation is implemented in both the NSCODE and CHAMPS solvers.

A last consideration can be made regarding the loss of accuracy in time linked to the sequential operator-splitting method. It was shown that an error is introduced by the method when the solution varies in time. However, when a steady-state is reached, the sequential operator-splitting method used in this case does not introduce an error because there is no time variation of the solution.

Indeed, for a steady-state to be reached by the filtered flow it is necessary that its value be equal to the value of the physical flow of the CFD solver, such that

$$W_n = \bar{W}_n = W_s. \tag{3.38}$$

When this happens, the action of the $e^{L\Delta t}$ operator on the filtered flow cancels itself and the relationship between $\bar{W}_n$ and $\bar{W}_{n+1}$ becomes

$$\bar{W}_{n+1} = \frac{1}{1+\chi\Delta}((I + \chi\Delta I) + (Ie^{-(\chi+\frac{1}{\Delta})\Delta t} - Ie^{-(\chi+\frac{1}{\Delta})\Delta t}))W_s = W_s. \tag{3.39}$$

Since the $e^{L\Delta t}$ operator is the only operator that can modify the value of $\bar{W}$, this represents the case where there is no variation in time for the filtered flow. When this equality is achieved, the action of the operator $e^{L\Delta t}$ on the physical flow W also has no effect, since it becomes

$$W_{n+1} = \frac{1}{1+\chi\Delta}((I + \chi\Delta I) + \chi\Delta(Ie^{-(\chi+\frac{1}{\Delta})\Delta t} - Ie^{-(\chi+\frac{1}{\Delta})\Delta t}))W_s = W_s. \tag{3.40}$$

If the value W_s is not a solution of the RANS equations, the solver will modify the value of the physical flow at the next iteration, removing the equality between the physical and filtered flow and meaning that a steady state was not actually reached. If however the solver also does not modify the value W_s, then the field is a solution of the equations. The operator $e^{L\Delta t}$ can be considered to vanish when a converged steady-state is obtained, indicating that it does not add new solutions compared with the original coupled formulation of SFD and that it does not introduce an additional error when the flow is steady in time.

3.2.3 Addition of periodic reset

A problem regularly encountered when using SFD, no matter the formulation used, is a slow rate of convergence exhibited by the solver compared to what could be expected for a similar case with the same parameters without SFD. In the cases presented in this work, a phenomenon observed was particularly a decrease of the initial convergence rate after a certain number of iterations.

This behavior is not surprising, since the modification of the eigenvalues of the system caused by the addition of SFD has been demonstrated mathematically [38] to reduce the damping of already stable eigenvalues associated with low frequencies. This is problematic from a practical point of view. The reduction of convergence rate varies when different parameters are used, and as observed in the numerical results of this work, even a parametric sweep aimed at optimizing the selection of the χ and Δ parameters leads to a pair of parameters exhibiting this convergence rate reduction. Such a sweep also reveals that many pairs of parameters can be suitable to stabilize the same test case but that among the suitable ones, the parameter pairs with the higher χ and Δ value present slower convergence. This is expected since an increase in these parameters results respectively in the filtered flow having a larger influence on the physical flow and on the filtered flow varying at a slower rate. In both cases, it could be expected that the convergence rate would be negatively impacted by the slow temporal variation of the filtered flow.

To counteract this phenomenon, an addition to the SFD formulations presented in the literature is proposed. An additional step is added to the SFD algorithm, consisting in periodically "resetting" the value of the filtered version of the flow field to the exact current

value of the physical flow field. The number of iterations between these "resets" is determined by the user as an input. This new input parameter is called the "r" parameter.

The goal of this modification is to avoid or minimize the convergence rate decrease associated with the use of SFD by directly changing the values of the filtered flow to what is hoped to be a better approximation of the solution corresponding to the partially converged physical flow. This can also be seen as restarting the solving algorithm with different initial values for the filtered flow, which should not be problematic in itself: Akervik et al. [24] specifically highlights the fact that the initial value of the filtered flow can be set arbitrarily without preventing convergence when using SFD as an advantage of the method.

The new resulting algorithm will not be repeated here entirely, because it consists in the same iterative algorithms presented for encapsulated SFD and coupled SFD, with the difference that for the n^{th} iteration, where n is a multiple of r, an additional step is done at the end of the iteration, which is defined as

$$\begin{pmatrix} W_{n+1} \\ \bar{W}_{n+1} \end{pmatrix} = \begin{pmatrix} W_{n+1} \\ W_{n+1} \end{pmatrix} \qquad n = [r, 2r, 3r, ...]. \tag{3.41}$$

This matrix definition highlights the fact that this additional step is very simple both from a mathematical and computational point of view. The only action required is a copy of an array of values and as such the additional computational time required to complete this additional step is negligible. The added function to complete this task is also very easy to implement.

3.2.4 Parameters selection

An important aspect to consider when using SFD is the selection of the parameters χ and Δ. These parameters can be selected with a process of trial and error or a more structured parametric sweep, but these methods require time to conduct multiple runs of the solver. These approaches can be made slightly more efficient by using educated guesses on suitable values of the parameters based on experience with the method.

Akervik et al. [24] give such a methodology based on their experience. If the eigenvalue of the unstable mode is unknown and can't be obtained, the frequency exhibited by the oscillating flow, ω_{flow} can be used. The Δ parameter should then be set to an approximate value of $\frac{2}{\omega_{flow}}$. The χ parameter is then set to an approximate value of $\frac{1}{\Delta}$.

The selection of the parameters can be improved by knowing the eigenvalue corresponding to the dominant unstable phenomenon. This eigenvalue is formulated as

$$\mu_o = \mu_{or} + i\mu_{oi} \tag{3.42}$$

where the real part of the eigenvalue represents the growth rate of the associated eigenmode and the imaginary part represents its frequency. This information can be used to improve the selection of the parameters of SFD. Akervik et al. [24] give additional indications for their general experience-based guidelines when this eigenvalue is known. The relationship for the Δ parameter can still be used with the imaginary part of the eigenvalue used instead of the frequency of the unstable phenomenon. Knowing the growth rate of the phenomenon, the χ value should be set as $\mu_{or} < \chi < \mu_{or} + (1/\Delta)$.

While this method of parameter selection can be useful for a single case or a case where not much information is known, a more advanced detailed methodology using the unstable eigenvalue to approximate the dynamics of the flow field can be used.

An approach used in this work is to approximate the complex flow problem with a simple scalar problem containing only the same unstable eigenvalue, since this unstable eigenvalue dominates the evolution of the flow field. The effect of SFD on this simple problem can then be used to represent the effect of SFD on the flow evolution. Jordi et al. [44] presented such a method with their encapsulated SFD formulation.

Assuming that we know the dominant unstable eigenvalue μ_o, we will use the simple 1-D problem

$$\dot{W} = \mu_o W \tag{3.43}$$

where μ_o is a constant number that can be complex. The solution to this problem for the evolution over the time span Δt from W_n to W_{n+1} is

$$W_{n+1} - W_n = e^{\mu_o \Delta t}. \tag{3.44}$$

The dynamic of this problem is driven by the value of μ_o which is equivalent to a unique eigenvalue of the problem. For the problem to converge toward a steady state, the real part of μ_o must be smaller than 0. Assuming that μ_o has a positive real part, the problem will

not converge toward a steady solution. Additionally, if μ_o has an imaginary part that is not equal to 0, it will present oscillations. In these conditions, we can apply SFD to the problem.

The mathematical effect of SFD is not the same depending on the implementation used between the original coupled SFD and the encapsulated SFD. Jordi et al. [44] use the matrix multiplication of the encapsulated SFD to conduct their analysis presented below.

To simplify the analysis, the evolution in time of the scalar problem without SFD will be represented by the analytical solution presented above. This corresponds to the case of an exact solver and removes possible numerical effects coming from the spatial and temporal schemes. Following this, the evolution between two iterations with SFD corresponds to a multiplication by the matrices of the two sub-problems as presented in Sec. 3.2.2, which results in the 2x2 matrix

$$\begin{bmatrix} \frac{1.0\left(\Delta\chi e^{\Delta t\left(-1.0\chi-\frac{1.0}{\Delta}\right)}+1.0\right)e^{\Delta t\mu_o}}{\Delta\chi+1.0} & \frac{1.0\left(-\Delta\chi e^{\Delta t\left(-1.0\chi-\frac{1.0}{\Delta}\right)}+\Delta\chi\right)}{\Delta\chi+1.0} \\ \frac{1.0\left(1.0-e^{\Delta t\left(-1.0\chi-\frac{1.0}{\Delta}\right)}\right)e^{\Delta t\mu_o}}{\Delta\chi+1.0} & \frac{1.0\left(\Delta\chi+e^{\Delta t\left(-1.0\chi-\frac{1.0}{\Delta}\right)}\right)}{\Delta\chi+1.0} \end{bmatrix}. \tag{3.45}$$

The condition for the system to converge toward a steady solution is now that the two eigenvalues of this matrix $\lambda_{e1,e2}$ must have a norm $|\lambda_{e1,e2}|$ smaller than 1.0. These eigenvalues can be calculated analytically and result in the expression

$$\begin{aligned} \lambda_{e1,e2} = & \\ \pm & \frac{\sqrt{-4\left(\Delta\chi+1\right)^2 e^{\Delta t\left(\mu_o+\frac{\Delta\chi+1}{\Delta}\right)}+\left(\Delta\chi e^{\Delta t\mu_o}+\Delta\chi e^{\Delta t\left(\chi+\frac{1}{\Delta}\right)}+e^{\Delta t\left(\chi+\mu_o+\frac{1}{\Delta}\right)}+1\right)^2}e^{-\frac{\Delta t}{\Delta}}e^{-\Delta t\chi}}{2\left(\Delta\chi+1\right)} \\ & + \frac{\left(\Delta\chi e^{\Delta t\mu_o}+\Delta\chi e^{\frac{\Delta t(\Delta\chi+1)}{\Delta}}+e^{\frac{\Delta t(\Delta\chi+\Delta\mu_o+1)}{\Delta}}+1\right)e^{-\Delta t\left(\chi+\frac{1}{\Delta}\right)}}{2\left(\Delta\chi+1\right)}. \end{aligned} \tag{3.46}$$

These eigenvalues are dependent on the variables $\chi, \Delta, \Delta t$ and μ_o. The first two variables are provided by the user and the two last ones are dependent on the original CFD solver. We can then apply an optimization algorithm on these equations to minimize both values $|\lambda_{e1,e2}|$ to maximize the damping of the unstable phenomenon.

This use of the encapsulated formulation is the one used by Jordi et al. [44] but is not very practical in the context of this work. The main reason for this is the fact that the time step Δt is present in the eigenvalues definition. This is not a problem when a global time step is used across the whole domain, but implies a lot of additional calculations for a solver using a local time step for each cell such as the steady state solvers used in this work.

To avoid computing the optimization problem presented above for each cell separately, the analysis of the modification of the eigenvalues when using the coupled SFD formulation is used. In this case, the original problem is once again approximated on a 1-D problem, using the dominant unstable eigenvalue μ_o of the Jacobian matrix $\frac{\partial R}{\partial W}$ which dominates the evolution of the flow in time. The resulting system of equation is

$$\begin{bmatrix} \dot{W} \\ \dot{\bar{W}} \end{bmatrix} = \begin{bmatrix} \mu_o - \chi & \chi \\ \frac{1}{\Delta} & \frac{-1}{\Delta} \end{bmatrix} \begin{bmatrix} W \\ \bar{W} \end{bmatrix} \tag{3.47}$$

which is similar to the system presented in Eq. 3.6 with the function representing the solver $f(W)$ replaced by the unstable eigenvalue μ_o. This 2x2 matrix will allow the system to converge toward a steady solution if both of its eigenvalues $\mu_{c1,c2}$ have a real part that is negative. These eigenvalues can once again be calculated analytically. The result is

$$\mu_{c1,c2} = -\frac{\Delta\chi - \Delta\mu_o + 1}{2\Delta} \pm \frac{\sqrt{\Delta^2\chi^2 - 2\Delta^2\chi\mu_o + \Delta^2\mu_o^2 + 2\Delta\chi + 2\Delta\mu_o + 1}}{2\Delta}. \tag{3.48}$$

This formulation of the resulting eigenvalue is equivalent to the one presented by Akervik et al. [24] with the difference that in the referenced work, the eigenvalues calculated are multiplied by -i and called the complex eigenvalues. In a similar approach as for the encapsulated formulation, this relationship between the original eigenvalue and the eigenvalue with SFD can be used with an optimization algorithm to maximize the damping of the original unstable eigenvalue. In this case, this means having a negative value as large as possible for the real parts of the new eigenvalues.

When comparing the modified eigenvalues obtained with the two methods, one important difference is that the eigenvalues obtained for the encapsulated formulation are for the matrix that advances the problem iteratively in time while the ones obtained for the coupled formulation are for the matrix defining the differential equation system. This difference makes it necessary to do an additional calculation to compare them. They can be related by bringing the encapsulated eigenvalues $\lambda_{e1,e2}$ in the differential referential with

$$\mu_{e1,e2} = \frac{ln(\lambda_{e1,e2})}{\Delta t} \tag{3.49}$$

in which case they can be compared with $\mu_{c1,c2}$ and the condition of stability is a real part smaller than 0. The eigenvalues $\mu_{c1,c2}$ can also be brought in the time referential with

$$\lambda_{c1,c2} = e^{\mu_{c1,c2}\Delta t} \tag{3.50}$$

in which they can be compared with $\lambda_{e1,e2}$ and the condition of stability is a norm smaller than 1.

When numerically comparing the eigenvalues obtained from the two formulations, it is possible to observe that for small time step values the two eigenvalues are close. However, as the time step Δt increases, the difference between the eigenvalues becomes important. This behaviour is illustrated in Fig. 3.1 where as an example the real part of the eigenvalues $\mu_{c1,c2}$ and $\mu_{e1,e2}$ are pictured for values of $\mu_o = 1.5 + 10i$, $\chi = 5.35$, $\Delta = 0.2$ for various Δt time step values.

To better understand the behavior of the encapsulated formulation's eigenvalues with a large time step, it is possible to use a simplified 1-D matrix by using the assumption that the term $e^{\Delta t(-1.0\chi - \frac{1.0}{\Delta})}$ becomes dominated by the large value of Δt and tends toward 0. This happens if the time step Δt is larger by order of magnitudes than the inverse of the $(-1.0\chi - \frac{1.0}{\Delta})$ term. The matrix representing an iteration of the 1-D problem then becomes

$$\begin{bmatrix} \frac{e^{\Delta t\mu_o}}{\Delta\chi+1.0} & \frac{\Delta\chi}{\Delta\chi+1.0} \\ \frac{e^{\Delta t\mu_o}}{\Delta\chi+1.0} & \frac{\Delta\chi}{\Delta\chi+1.0} \end{bmatrix} \tag{3.51}$$

which has only one eigenvalue

$$\frac{\Delta\chi + e^{\Delta t\mu_o}}{\Delta\chi + 1}. \tag{3.52}$$

The condition to ensure stability is that this eigenvalue needs to have a norm smaller than 1. However with the assumption that a large time step is used, it can be seen that this eigenvalue will be dominated by the term $e^{\Delta t\mu_o}$, which corresponds to the behavior of the original problem. This can be observed in Fig. 3.2, where the eigenvalues $\mu_{e1,e2}$ and $\mu_{c1,c2}$ are pictured for the same example values as in Fig. 3.1. When the time step is augmented

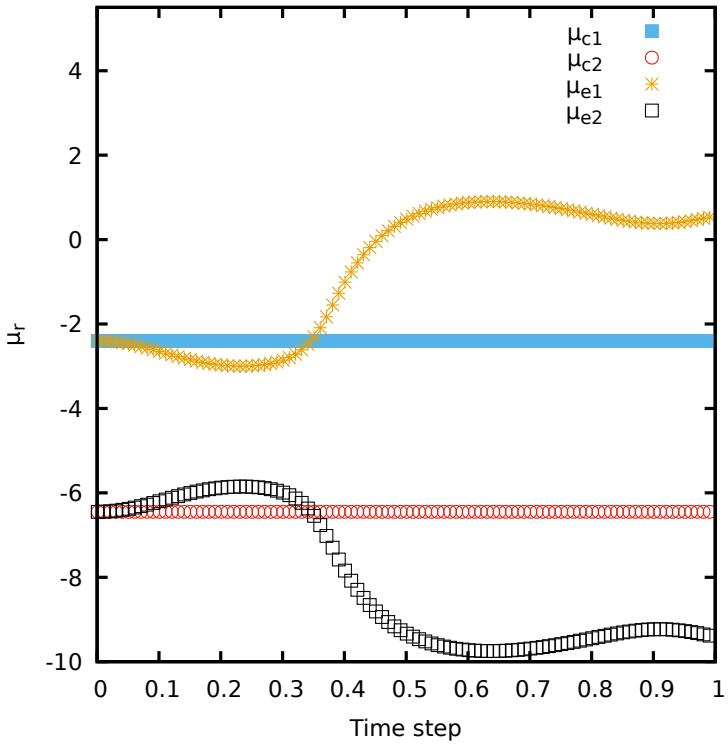

Figure 3.1 Comparison of modified eigenvalues from the encapsulated and coupled formulations of SFD for various time steps

further, it is possible to see that the real part of the eigenvalues linked to the encapsulated formulation tends toward the real part of the original eigenvalue that is set as $\mu_{or} = 1.5$.

This means that if the original problem did not converge toward a steady-state solution, using the encapsulated formulation of SFD with a large time step to stabilize the problem has a high chance of failure. From this observation, it is concluded that special care must be taken concerning stability when using encapsulated SFD in conjunction with a large time step. This situation can potentially arise when using an implicit temporal scheme.

It is also decided based on this observation to use the eigenvalue analysis of the coupled SFD formulation to optimize the value of the χ and Δ parameters, both when using the encapsulated and coupled formulation of SFD. The reasoning for this choice is that the need to consider the time step in the encapsulated formulation's eigenvalues would result in an impractically high number of required calculations since a separate optimization would be needed for each cell in the domain. In addition, the expression of the coupled formulation's eigenvalue has fewer terms and as such has a lower computational cost. Finally, the use of

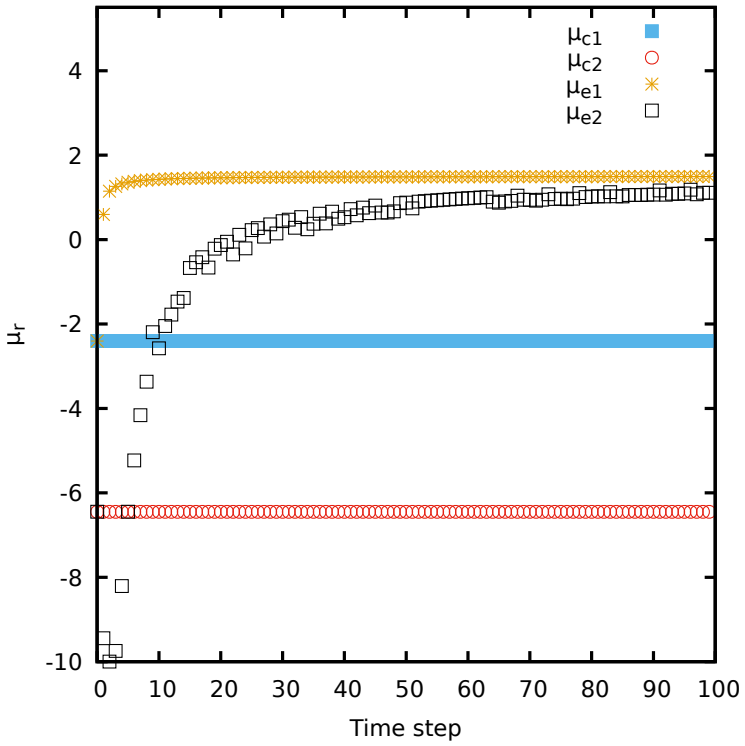

Figure 3.2 Comparison of modified eigenvalues from the encapsulated and coupled formulations of SFD with large time steps

the coupled formulation has been shown to be a good approximation of the encapsulated formulation's eigenvalues when using a small time step. The higher error encountered when using a longer time step is not considered limiting, since it has been shown earlier that the use of a large time step with the encapsulated formulation of SFD is not desirable.

A last consideration is given to the effect of the parameters χ and Δ on the eigenvalues that are already stable. While in the presence of an unsteady phenomenon without SFD the convergence of the flow is dominated by the eigenvalue with the largest positive real part, in the case where no eigenvalue has a positive real part the least damped eigenvalue is the one with a negative real part closest to zero. In a graph using the X-axis to display the imaginary part and the Y-axis to display the real part of a number, the eigenvalue at the most upward position would then be the one limiting the convergence of the problem.

While the effect of SFD is to reduce the real part of eigenvalues with a sufficiently high imaginary part by damping oscillations, its effect on eigenvalues with an imaginary part sufficiently small can potentially create new modified eigenvalues for which the real part is

closer to zero than the original. This can be observed in Fig. 3.3 in which the new modified eigenvalues $\mu_{c1,c2}$ are shown for one unstable original eigenvalue with a real part of 1.5 and one stable eigenvalue with a real part of -1.0. The values of the parameters are set to $\chi = 5.35$ and $\Delta = 0.2$ as an example. The imaginary part of the original eigenvalues is varied to show the effect for various eigenvalues with the same real part. Arrows are used to link the original eigenvalues to their modified pair of eigenvalues with SFD for the cases of eigenvalues with a large or small imaginary part in both the stable and unstable cases.

Globally it can be seen that an eigenvalue with a smaller imaginary part will be less damped by SFD than an eigenvalue with a large imaginary part, and can even become less damped than it was originally without SFD. Casacuberta et al. [38] demonstrated however that SFD will never create an unstable eigenvalue from an originally stable eigenvalue.

This dependency of the real part of the modified eigenvalues relative to the imaginary part of the original eigenvalues highlights one problem with considering only the unstable eigenvalue in a 1-D system to optimize the parameters. Taking as an example Fig. 3.3, let us consider the case where these χ and Δ parameters are used on a system with an eigenvalue of $1.5 - 30.0i$ and a stable eigenvalue of $-1.0 + 6.0i$. Both of these eigenvalues are pictured in Fig. 3.3 with arrows pointing to their corresponding modified eigenvalues in the augmented system. We can see that the eigenvalue limiting the convergence after applying SFD originates from the originally stable eigenvalue.

This means that only optimizing the χ and Δ parameters to maximize the damping of the most unstable eigenvalue will usually result in a sub-optimal choice of parameters when considering the convergence rate of the problem since other less damped eigenvalues will then dominate the convergence rate. Some authors such as Cunha et al. [45] and Casacuberta et al. [38] have used methodologies to consider such eigenvalues in their optimization. However, these methodologies come with drawbacks. In the case of Cunha et al. more eigenvalues need to be evaluated without knowing in advance which one will be the most limiting in term of convergence rate. In the case of Casacuberta et al., the limiting eigenvalue is evaluated by observing the behavior of the stabilized flow which can be complex without manual intervention.

In the context of this work, the approach chosen is to use the simplified model only considering the unstable eigenvalue. The first reason for this approach is the fact that as presented in Sec. 3.3 and 3.4, the global stability analysis method used to identify the unstable eigenvalue

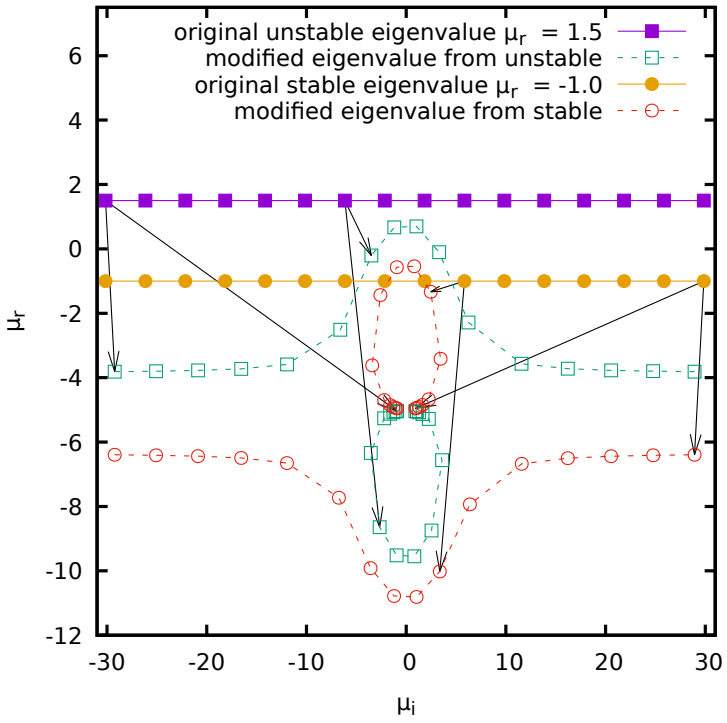

Figure 3.3 Visualization of the new eigenvalues created from unstable and stable eigenvalues when using SFD, $\chi = 5.35$, $\Delta = 0.2$

is sometimes used on a partially converged flow which limits the accuracy of the estimation of the unstable eigenvalue. Since SFD can't make stable eigenvalues unstable, it is preferable to prioritize the damping of unstable eigenvalues to ensure that no unstable eigenvalues will remain when using approximations of the unstable eigenvalue. In addition, the complexity associated with the identification of the most limiting stable eigenvalue results in a more computationally expensive algorithm. Finally, the addition of the periodic reset presented in Sec. 3.2.3 was able to drastically diminish the problem of the convergence rate being reduced by SFD. The problem of a slightly sub-optimal rate of convergence consequently became less limiting compared with the other arguments presented previously.

3.3 Global Stability Analysis

The analysis of the modification of the dominant eigenvalue presented in Sec. 3.2.4 requires knowing the dominant unstable eigenvalue of the flow to be useful. Multiple methods exist to obtain this eigenvalue, however the method used in this work is global stability analysis. The reasons for this choice compared with other methods mentioned in the literature review is that

compared to the DMD method used by Cunha et al. [45], the global stability analysis method is not influenced by non-linear effects which allows it to focus on the small perturbation domain associated with the onset of instability. From an implementation standpoint, the global stability analysis method was also associated with less risk during development since it can leverage functions already present in the solver to calculate necessary values and since support during development could be provided by a member of the research team already familiar with the method. This would not have been the case for the DMD method. Moreover, the global stability analysis method was preferred to the "flow unleash" method of Casacuberta et al. [38] because it requires fewer manual operations which can be limiting when using these methods in an industrial context. The global stability analysis method is implemented for the laminar equations in the NSCODE solver.

The general RANS equations solved in this work have already been presented in Eq. 1.13. These equations are nonlinear because of the term $\overrightarrow{R}(\vec{W})$. We want to analyse the behaviour of these equations for small perturbations, linearized around a value $\vec{W}_s$ such that $\vec{W}_l = \vec{W}_s + \Delta\vec{W}$. The nonlinear term $\overrightarrow{R}(\vec{W})$ can be linearized as

$$\overrightarrow{R}(\vec{W}) = \overrightarrow{R}(\vec{W}_s) + \frac{\partial \overrightarrow{R}(\vec{W}_s)}{\partial W}(\Delta W). \tag{3.53}$$

The new linearized equation is now

$$\Omega\frac{\partial \vec{W}_l}{\partial t} = \Omega\frac{\partial \vec{W}_s}{\partial t} + \Omega\frac{\partial \Delta\vec{W}}{\partial t} = -\overrightarrow{R}(\vec{W}_s) - \frac{\partial \overrightarrow{R}(\vec{W}_s)}{\partial W}(\Delta W). \tag{3.54}$$

From the original equation we know that

$$\Omega\frac{\partial \vec{W}_s}{\partial t} = -\overrightarrow{R}(\vec{W}_s) \tag{3.55}$$

and Eq. 3.54 can be simplified to

$$\Omega\frac{\partial \Delta\vec{W}}{\partial t} = -\frac{\partial \overrightarrow{R}(\vec{W}_s)}{\partial \vec{W}}(\Delta\vec{W}). \tag{3.56}$$

This last equation is now a linear differential matrix equation, and the behavior of the solution can be analyzed with the eigenvalue of the matrix $\frac{\partial \overrightarrow{R}(\vec{W}_s)}{\partial \vec{W}}$ which has constant coefficients. It should be stressed here that this matrix represents the entire field. It is a very large square matrix with a size of 5 times the total number of cells in the row and column

directions for a tridimensional laminar flow since in this case 5 conservative variables are solved. Global stability analysis is based on the idea of assembling this matrix, called the global Jacobian matrix, and computing its eigenvalues to characterize the evolution of the flow in the range of small perturbations. In this case, the Jacobian matrix is evaluated with finite difference to approximate it numerically as $\frac{\Delta \vec{R}(\vec{W}_s)}{\Delta \vec{W}_s}$.

The first step to implement this method is the calculation of the Jacobian matrix. To assemble this matrix numerically by finite difference, each variable of each cell in the domain must be perturbed and the effect of each of those perturbations on the residual of every cell in the domain must be stored. This would theoretically result in a very large number of perturbations and subsequent residual calculations. In practice, it is possible to greatly diminish the required computation to assemble this matrix by considering how a cell affects the residual of another.

The case of the NSCODE solver will be used to demonstrate this. The calculation of the residual in each cell in this structured solver only takes into account the values of the cells directly in contact with the cell and the cells one further cell away in each principal direction "i" and "j". The area affected, which will be referred from now on as the stencil of the cell, is pictured in Fig. 3.4 for two cells identified with "X" marks. Knowing that only the cells in this area around a perturbed cell will experience a variation of their residual, time can be saved by only storing the variation in these cells and ignoring the others since the stored value will necessarily be 0.

With this information, it is also possible to perturb multiple cells at the same time as long as their stencils do not overlap and gather the difference in the residual in each of the cells in their respective stencil. This saves a great amount of computational time, since these operations are done through functions already present in the solver that normally already act on the entire domain simultaneously. With these strategies, instead of requiring to compute a function to perturb the field and subsequently measure the residual for each variable multiplied by the number of cells, the required steps can theoretically be as low as 13 steps multiplied by the number of variables in the optimal case. In practice, the amount of steps required is usually greater because of the cells near the boundaries that have incomplete stencils.

To identify with which pattern and in which order the cells will be perturbed, an in-house program is previously run on the meshes. This program iteratively selects as many cells

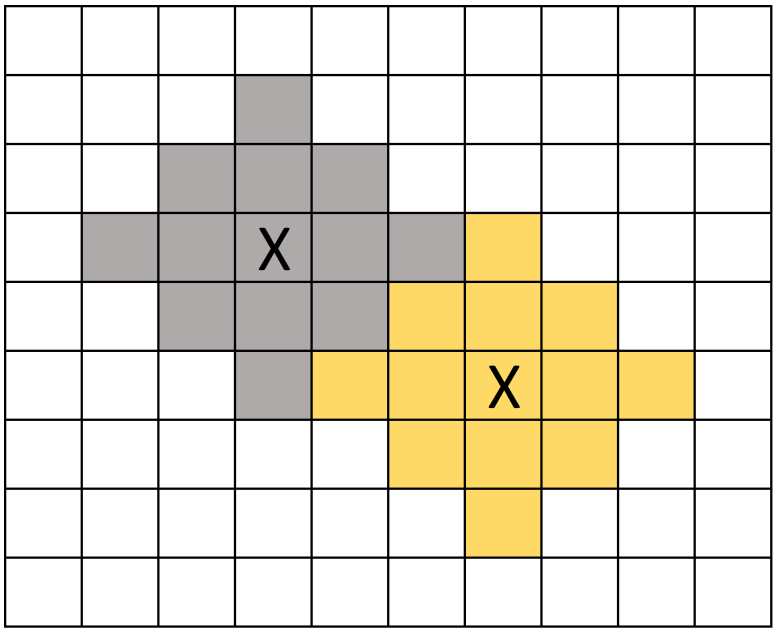

Figure 3.4 Adjacent stencils of two cells in the case of the structured solver NSCODE

as possible for which none of their stencils overlap and identifies them as part of the same perturbation step. These cells are then removed from the search algorithm and the operation is repeated until all cells are part of one perturbation step. The patterns in these steps are stored in files provided to the solver as input to be used in the flow perturbation function.

After the patterns of perturbations are established, the perturbation itself can be generated. This perturbation must be of a small value to remain in the linear domain of the analysis. In the case of the global stability analysis implemented in NSCODE, the perturbations applied all have a value of 1.0e-6. No sensitivity study was done on this constant value. To get achieve second order, a central difference is used, which means that all the cells are perturbed twice: once by adding the perturbation value and another time by subtracting it. The result is then used to compute the finite difference, calculated for each cell at position (o,p) for the residual of each variable j in the stencil of the perturbed cell at position (n,m) for the perturbation of each variable i

$$\frac{\Delta R_j^{o,p}}{\Delta W_i^{n,m}} = \frac{R_j^{o,p}(W_i^{n,m} + \epsilon) - R_j^{o,p}(W_i^{n,m} - \epsilon)}{2.0 \times \epsilon}, \qquad \epsilon = 1.0 \times 10^{-6}. \tag{3.57}$$

These finite difference values are then stored with their corresponding location in the complete Jacobian matrix. When all perturbations and residual calculations have been com-

pleted, the Jacobian matrix is obtained and the next step is to compute its eigenvalues. Since the Jacobian matrix is a very large matrix, it would be impractical to compute all of its eigenvalues and subsequently identify the dominant unstable eigenvalue among them. To remedy this problem, the external function libraries PETSc and SLEPc are used. These libraries contain solver functions specifically designed to compute a specific number of eigenvalues from a large sparse matrix according to specific requirements.

In this implementation, an Arnoldi eigensolver is used in conjunction with a shift-and-inverse spectral transformation. The shift-and-invert spectral transformation allows to specify a target value around which to search for the eigenvalue. This allows us to specify to the solver that it should search for eigenvalues with positive real parts and relatively high imaginary parts. In particular, if an approximation of the expected eigenvalue is known, either because a previous global stability analysis was already conducted or because of information from the literature, this expected eigenvalue can be used to accelerate the convergence of the eigensolver thanks to a better initial guess. When the eigensolver has converged to the required eigenvalue, the global stability analysis is complete and the obtained eigenvalue can be used to characterize the flow [59].

3.4 Adaptive selective frequency damping

The previous subsections have presented how to calculate the dominant unstable eigenvalue characterizing the instability in the flow and how to calculate the effect of the χ and Δ parameters when applying SFD on this eigenvalue. Both of these methods can be coupled to optimize the selection of the parameters on a test case. This approach was presented by Jordi et al. [44] and is called by these authors the adaptive SFD algorithm. The adaptive SFD algorithm implemented in this work is similar to the one presented by these authors but with some differences that will be described in this section.

This algorithm consists in first letting the solver complete a certain number (selected by the user before execution) of iterations, either without SFD or with SFD using parameters initially selected by the user. After these iterations are completed, a global stability analysis, as presented in Sec. 3.3 is conducted on the partially converged flow. This first global stability takes as inputs the required precision for the eigenvalue found and an initial guess to set the value of the shift-and-invert spectral transformation. In this case since the goal is to identify the unstable eigenvalue, this guess should have a positive real part.

The result of this global stability analysis is an unstable eigenvalue that is used to conduct a basic optimization of the χ and Δ parameters. The analysis is based on the modification of the eigenvalues presented in Sec. 3.2.4. The dominant eigenvalue considered is the one found with the previous global stability analysis. The modification of this eigenvalue according to the analysis based on the coupled formulation of SFD is used since it has a lower computational cost and is considered a good approximation of the encapsulated formulation of SFD when a small time step is used, which should be the case to limit the error in time associated with this formulation. This differs from the original adaptive SFD algorithm of Jordi et al. [44] who used the encapsulated formulation in their 1-D model to analyze the modification of the eigenvalue.

The goal of the optimization is to select a couple of parameters to maximize the damping of the original eigenvalue, which means making the real parts of the two corresponding eigenvalues negative and as far from zero as possible. Multiple methods would be possible to conduct this optimization. In the case of this work, the optimization method used is a simple parametric sweep of various χ and Δ. The modified eigenvalues are evaluated iteratively for every pair of parameters. If both modified eigenvalues have a larger negative real part than the previous best result, the χ and Δ parameters replace the previous best pair. When the parametric sweep is complete, the best identified pair of parameters replaces the previous pair of parameters used.

The values of χ and Δ tested during the parametric sweep consist in 2000 values for each parameter, centered around the χ and Δ parameters that would be expected based on the empirical relation provided by Akervik et al. [24] presented in Sec. 3.2.4 as an initial guess. The boundaries for the tested values are a maximum of 5 times the initial guess and a minimum of 0,25% of the initial guess. This minimum allows the eigenvalue evaluation to consider cases where the parameters are almost negligible, which roughly corresponds to a case without SFD while avoiding testing a value of zero and an undefined division by zero. This simple optimization method is admittedly not particularly efficient, however since this step does not represent a significant computational cost, this choice is made to not add to the complexity of the whole algorithm.

Once this optimization is complete, the iterations of the solver are resumed while being stabilized by SFD, either with the encapsulated or coupled formulations, while using the identified optimal parameters to maximize the damping of the phenomenon. After a certain amount of iterations selected by the user prior to the execution, the global stability analysis

is once again conducted on the partially converged flow. The flow should now have a better convergence, and as such the eigenvalue found should be similar to the one of the previous global stability analysis but represent more accurately the unstable phenomenon. For this reason, the initial guess given to the shift-and-invert spectral transformation is the value of the unstable eigenvalue found in the previous global stability analysis. A new optimization of the χ and Δ parameters is then conducted in the same way as the first one.

This algorithm is repeated until a sufficient residual convergence criterion is reached. It was shown in Sec. 3.2 that while the original equations have a residual that can be used to evaluate the convergence of the solver, there also exists a residual that can be used to evaluate the convergence of the solver considering the equation of the low-pass filter. When both of these residuals reach a sufficient convergence, the global stability analysis and subsequent parameters optimization are not conducted anymore. This is because the flow is considered close enough to the solution, which means the unstable eigenvalue will not vary meaningfully and the parameter optimization would not give different results. In the case of the present algorithm, the criteria used is a residual convergence of 3 orders of magnitude.

The iterations of the solver with SFD are then continued until sufficient convergence of the flow equations is reached. The complete algorithm is represented schematically in Fig. 3.5 where the first convergence criteria to stop the solver iterations and the second convergence criteria to bypass the global stability analysis and parameter optimization are pictured.

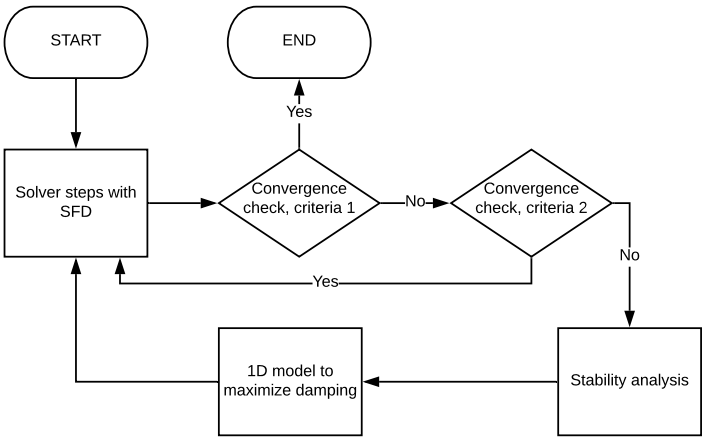

Figure 3.5 Schematical representation of the adaptive SFD algorithm implemented in NSCODE

CHAPTER 4 NUMERICAL RESULTS

This section contains the numerical experiments that were conducted during this research project to verify and validate the implementation of the instability recognition and stabilization in both the NSCODE solver and the CHAMPS solver. The results are compared with relevant results from the literature. An important point about the test cases presented in this section is that since the stated goal of the algorithm is to stabilize a RANS solver searching for a steady-state solution, a local time-stepping scheme is used to advance the equations in time unless stated otherwise. The test cases presented in the literature of stabilization with SFD are usually done with time-accurate simulations to get a representation of the unsteady phenomenon in time, with the notable exception of Richez et al. [22]. This difference in methodology does not affect the steady solution of the simulation and it is hypothesized that for small perturbations of the flow where a linearization can be used to represent its evolution, the use of local time-stepping does not prevent SFD to be effective.

4.1 Laminar cylinder

The laminar flow around a circular cylinder test case is a well-known case that results in unsteady vortex shedding for a range of low Reynolds number. This test case is first studied in NSCODE for a Reynolds number of 150, which is above the critical Reynolds number for the appearance of an instability in a laminar flow found in the literature. The Mach number used is 0.2 and the diameter of the cylinder is 1.0. Since this is a laminar flow case, no turbulence model is used. For this test, the temporal scheme is advanced using a hybrid 5 stage Runge-Kutta scheme. Moreover, the multigrid capabilities of NSCODE are used in this test case to reduce computational time, and so a multigrid algorithm of 3 levels in a W-cycle is used. The mesh used is a structured O-grid of 257x129 cells. The farfield is placed at 50 diameter length from the center of the mesh.

4.1.1 Unstabilized RANS simulation

To ensure the unsteady phenomenon is captured by the solver, the test case without stabilization is first run. A RANS simulation aiming to obtain a steady state solution is first conducted. As it can be seen in the resulting residual convergence and lift coefficient over iterations in Fig. 4.1a and Fig. 4.1b respectively, the solver is unable to converge to a steady solution. This can be explained by the instability of the unsteady phenomenon appearing in

these conditions.

A visualization of the flow field in Fig. 4.3 confirms the fact that the unsteady vortex shedding phenomenon is captured by the solver since the asymmetrical vortex shedding can be observed in the unconverged flow field.

4.1.2 Encapsulated SFD

To damp the unsteady phenomenon, the ESFD implementation in NSCODE is used. The χ and Δ parameters used are constant and respectively of value 0.1 and 14.826 with a reset of the low-pass time-filtered flow every 300 iterations. These values are chosen based on the experience of multiple testing and are used to validate that a steady-state flow can be obtained with a classical implementation with constant parameters. It can be observed in Fig. 4.4a that the solver is able to converge to machine accuracy with these parameters. The lift coefficient value obtained corresponds to the theoretical value of 0.0 for this symmetrical case as seen in Fig. 4.4b. A visualization of the flow solution in Fig. 4.6 confirms the fact that the steady solution reached does not show the vortex shedding behavior previously observed.

4.1.3 Unsteady RANS simulation

To further confirm that the vortex shedding phenomenon is encountered and to ensure the NSCODE solver is able to capture the unsteady phenomenon in a time-accurate scheme, a URANS simulation is conducted with the NSCODE solver on the same case with a Reynolds number of 100.0. The interest of this Reynolds number is the availability of similar URANS simulations in the literature for comparison.

The variation of the lift and drag coefficient with respect to time are displayed in Fig. 4.8. The Strouhal number of the oscillation is compared with the computational results of Rajani et al. [6] and the experimental results of Williamson [14] in Table. 4.1. While the mean drag coefficient of 1.3527 obtained differs by 1.3% from the one obtained by Rajani et al. of 1.3353, the Strouhal number agrees well with the literature. In addition, the development of the instability and the general behavior of the flow match the results of Rajani et al. for a similar simulation.

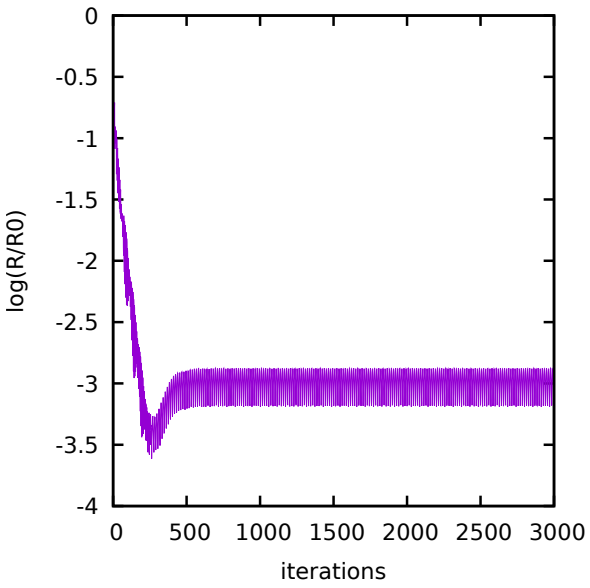

Residual convergence of the laminar cylinder case without SFD for a RANS simulation

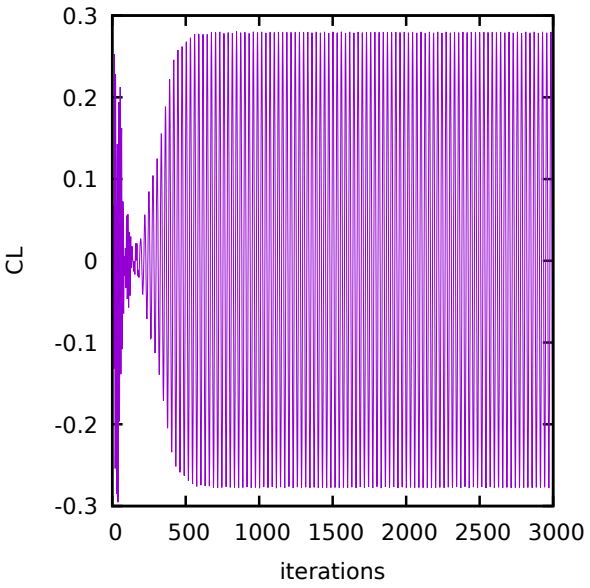

Lift coefficient of the laminar cylinder case without SFD for a RANS simulation

Figure 4.2 Evolution of NSCODE solver metrics during calculation of the laminar cylinder case without SFD

Table 4.1 Strouhal number of vortex shedding over laminar cylinder at Re=100.0 from NSCODE and literature

Provenance	Strouhal
NSCODE	0.1637
Rajani et al.	0.1569
Williamson	0.1643

4.1.4 Global stability analysis

To first validate the global stability analysis functionality implemented in NSCODE, a global stability analysis is run on a laminar flow case on the same cylinder. To allow a better comparison with the literature, the Reynolds number used for this simulation is 100.0. The base field used to run the global stability analysis is the steady state solution of the test case, which can be obtained by stabilizing the solver with constant parameters as mentioned in subsection 4.1.2. The eigenvalue obtained is $0.0277 \pm 0.171i$. The nondimensionalized corresponding value is then $0.117 \pm 0.721i$ This result is in good agreement with the results of Crouch et al. [2] and Jordi et al. [44] for a similar global stability analysis as shown in Table. 4.2.

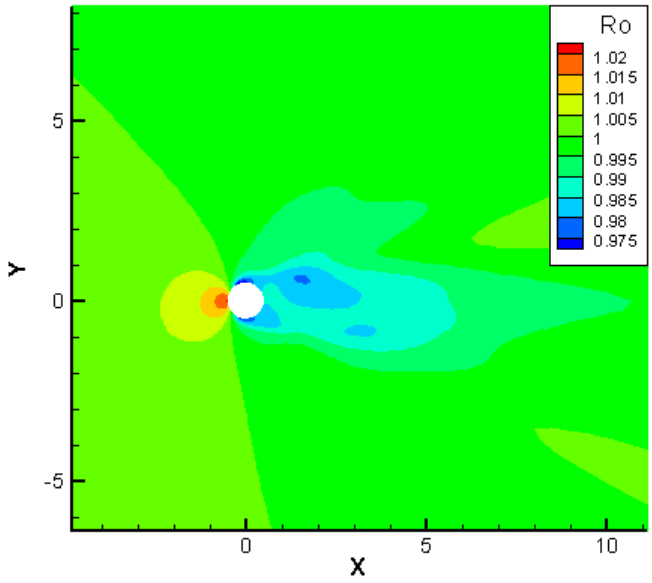

Figure 4.3 Flow density solution of laminar cylinder case at iteration 20 000 without SFD for a RANS simulation

Table 4.2 Nondimensional eigenvalues obtained from a global stability analysis from NSCODE and literature

Provenance	Eigenvalue
NSCODE	$0.117 \pm 0.721i$
Crouch et al.	$0.11 \pm 0.72i$
Jordi et al.	$0.127 \pm 0.741i$

The shape of the eigenmode associated with this unstable eigenvalue is also visualized. A comparison in Fig. 4.10 of the real part of the u-component with the result of Crouch et al. [2] shows good agreement for the shape of the eigenmode.

4.1.5 Adaptive SFD

To demonstrate the functionality of the adaptive SFD algorithm implemented in NSCODE, the algorithm is run on the test case for a Reynolds number of 150. The χ and Δ parameters used are initially set to 0 before the first global stability analysis. The global stability analysis is conducted every 300 iterations. The criteria for stopping the global stability analysis and freezing the SFD parameters is the residual of the low-pass time filter equation reaching a convergence of three orders of magnitude. To demonstrate the functionality of the periodic

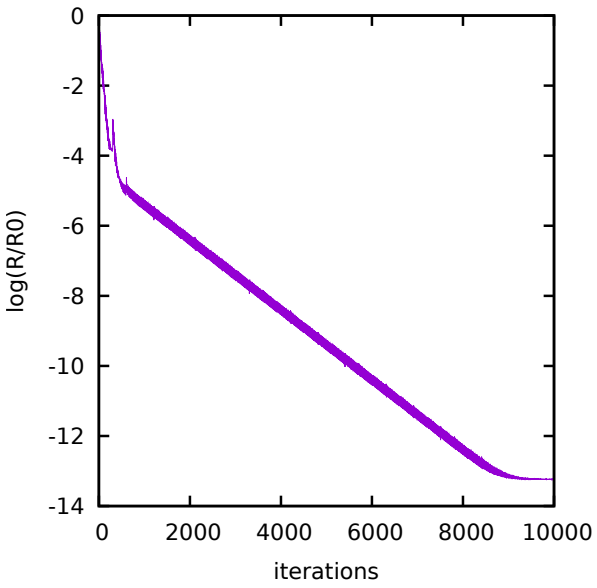

Residual convergence of the laminar cylinder case with ESFD for a RANS simulation

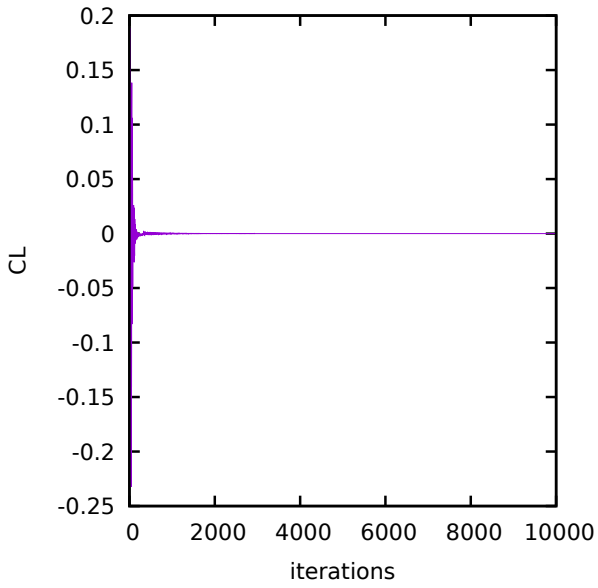

Lift coefficient of the laminar cylinder case with ESFD for a RANS simulation

Figure 4.5 Evolution of NSCODE solver metrics during calculation of the laminar cylinder case with ESFD

reset of the filtered flow, the case is run both without any periodic reset and with a periodic reset every 60 iterations. The resulting convergence of the solver is presented in Fig. 4.11 with the original unstabilized simulation for comparison purpose. It can first be assessed from this figure that the parameters selected by the adaptive SFD algorithm are indeed able to damp the oscillations coming from the unsteady phenomenon and to make the solver converge. However, it can be seen that the convergence rate with the selected χ and Δ parameters is impractically slow. The addition of the periodic reset of the low-pass filtered flow results in a significant increase in the convergence rate.

On the subject of the eigenvalues identified on the partially converged flow, the run without a periodic reset resulted in multiple subsequent calculations of eigenvalues since the slower convergence rate prevented the solver from reaching the convergence threshold to freeze the parameters. In total, 66 eigenvalues evaluations were conducted for this run. The nondimensional eigenvalues identified varied from $0.15265 \pm 0.69547i$ to 0.14955 ± 0.67199, converging toward this last value. In the case of the run with a periodic reset of the low-pass filtered flow, only 2 eigenvalues evaluations were necessary before sufficient convergence was reached to freeze the parameters. The nondimensional eigenvalues identified in this case varied between $0.14879 \pm 0.68133i$ and 0.14880 ± 0.67625. A subsequent global stability analysis was executed

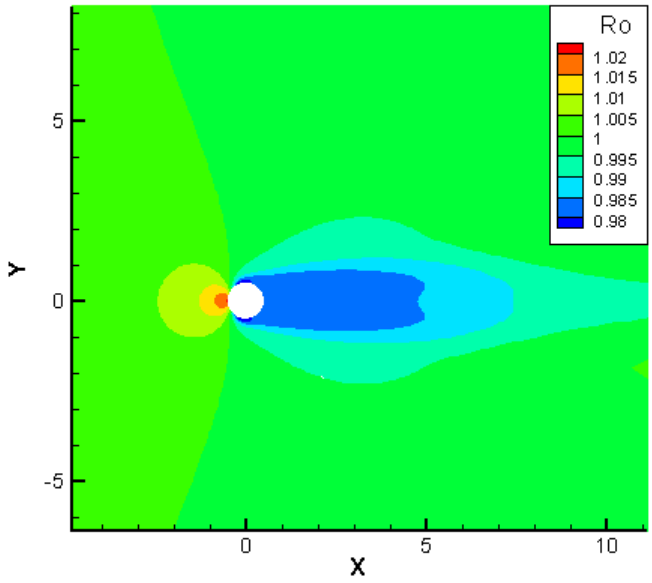

Figure 4.6 Flow density solution of laminar cylinder case at iteration 10 000 with ESFD for a RANS simulation

separately on the steady flow solution converged to machine accuracy which resulted in an eigenvalue of 0.14956 ± 0.67189.

These results highlight the fact that without a periodic reset the solver with SFD is able to converge to a solution where the physic of the unsteady phenomenon is not present in the flow, since the eigenvalue found without a periodic reset on the partially converged flow converges toward the expected value. They also show that the reset of the filtered flow alleviates the fact that the convergence of the solver then gets limited by the slow evolution of the filtered flow. This phenomenon can be observed in Fig. 4.12 where the lift coefficient evolution with respect to the iterations of the solver is shown with and without reset. SFD without reset results in the oscillations being damped, but also with the lift coefficient slowly converging toward the expected value of 0 after the oscillations are removed. The lift coefficient notably shows a bias toward a lower value when approaching the expected solution when no periodic reset is used, with this tendency being removed from the evolution of the lift coefficient when the periodic reset functionality is used.

The optimization of the χ and Δ parameters based on the eigenvalue found converged toward $\chi = 0.0995$ and $\Delta = 15.56$. These values correspond to a local minimum concerning

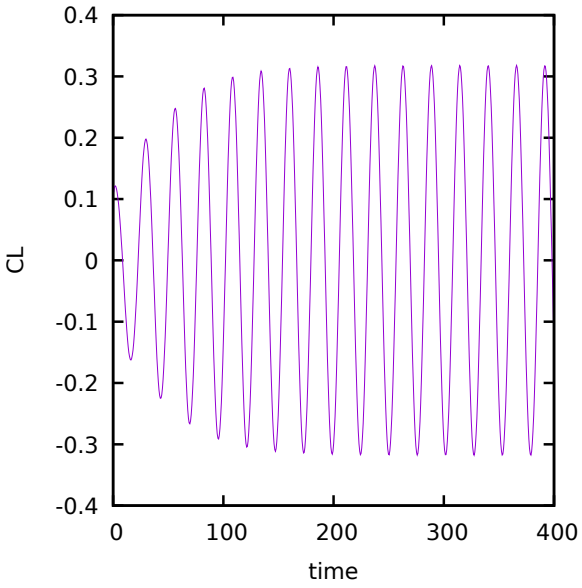

Lift coefficient of the laminar cylinder case for a URANS simulation

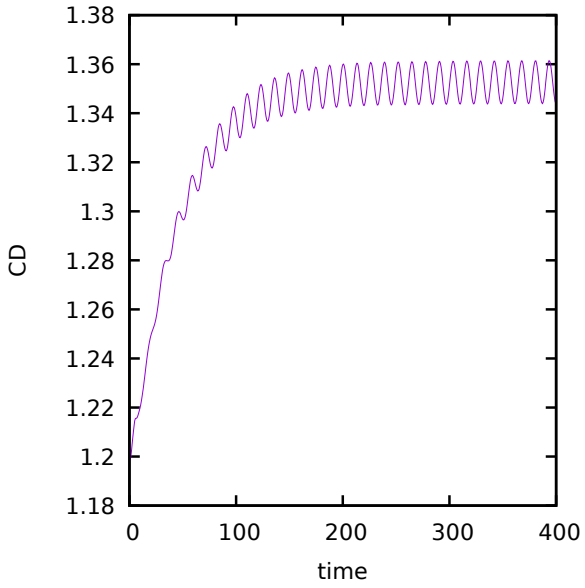

Drag coefficient of the laminar cylinder case for a URANS simulation

Figure 4.8 Evolution of NSCODE solver metrics for a URANS simulation of the laminar cylinder case

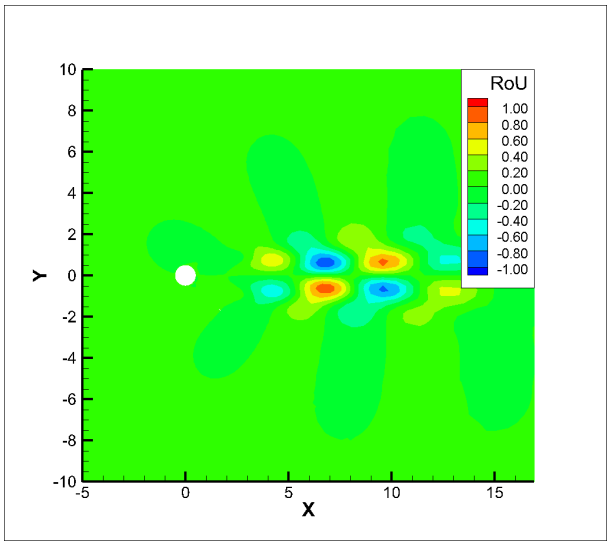

Conservative u-component eigenmode of laminar cylinder case from NSCODE global stability analysis

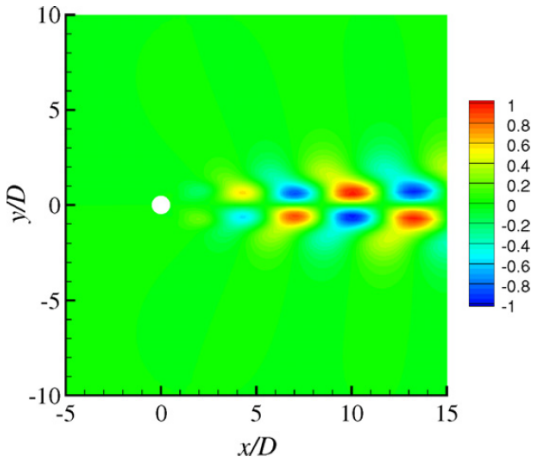

Conservative u-component eigenmode of laminar cylinder case reproduced from Crouch et al. global stability analysis [2]

Figure 4.10 Comparison of the conservative u-component of the eigenmode of laminar cylinder case from global stability analysis between NSCODE and Crouch et al. [2]

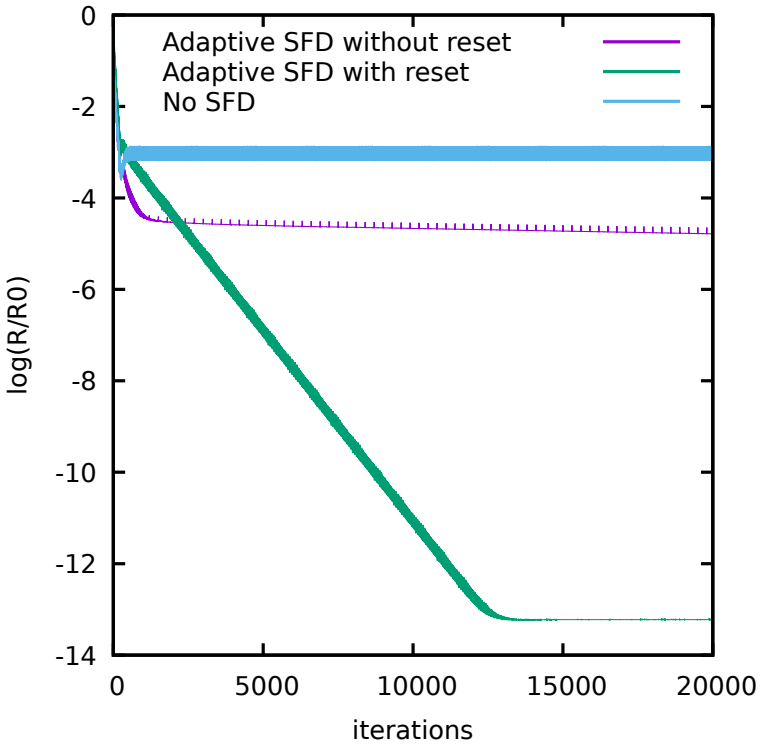

Figure 4.11 Comparison of residual convergence of the laminar cylinder case for a RANS simulation

the highest real part of the two modified eigenvalues, as shown in Fig. 4.13 which displays the values obtained when the algorithm conducted the parametric sweep for χ and Δ based on the eigenvalue obtained at the last global stability analysis.

4.1.6 Comparison of encapsulated and coupled formulations

The previous results presented for the cylinder case were obtained with NSCODE. However, as it was mentioned in Sec. 3.2, only the encapsulated SFD formulation was implemented in the NSCODE solver. Since both the original coupled formulation and the encapsulated formulation of SFD were implemented in the CHAMPS solver, this solver is now used to compare the stability of both implementations on the same case of vortex shedding in a laminar flow around a cylinder. The flow conditions used are a Reynolds number of 150.0 and a Mach number of 0.2. The solver used is an implicit LU-SGS solver to allow the use of large Courant-Friedrichs-Lewy (CFL) numbers. The mesh used for this case is an unstructured mesh of 54850 cells either of triangular or quadrilateral shape in which the wake of the cylinder is specifically refined to study the behavior of vortex shedding.

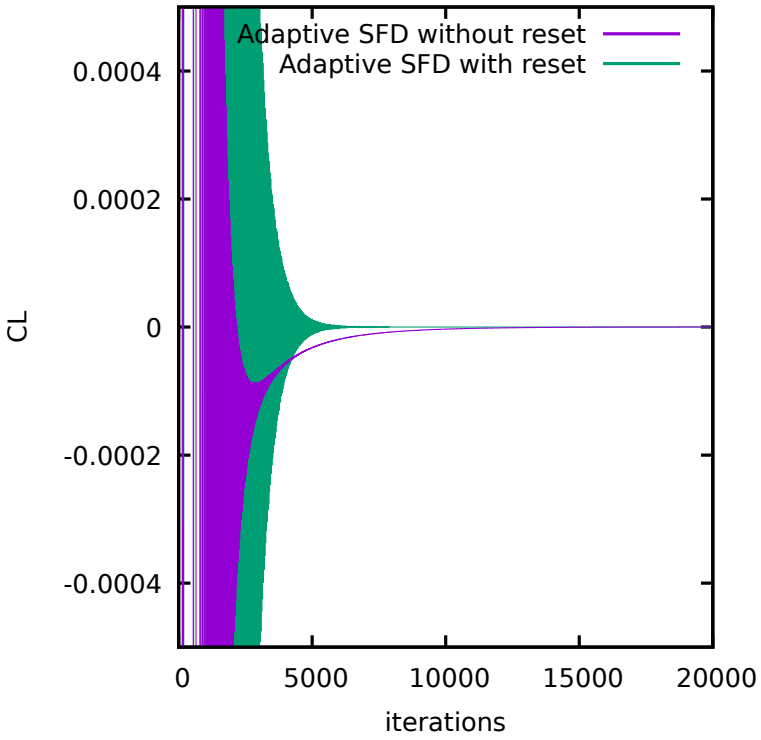

Figure 4.12 Comparison of lift coefficient of the laminar cylinder case for a RANS simulation

Since the goal in this section is only the comparison of the stability of both formulations, the methodology used is based on the resulting convergence after a predetermined amount of iterations for both formulations with the same parameters. The case is first tested with the solver without SFD to observe the value of the residual norm reached before the instability stops a further reduction of the residual. A sufficient amount of iterations is used so that a limit-cycle oscillation state is reached. The same test case is then computed with both formulations of SFD on the same amount of iterations with a parametric sweep of the χ and Δ values. The parameter values tested are separated by an order of magnitude each to cover a large range of values. The tested parameter values for χ and Δ are 0.001, 0.01, 0.1, 1.0, 10.0, 100.0 and 1000.0. After the same amount of iterations that was previously used on the case without SFD is reached, the solver is stopped. This test is done for CFL numbers of 5.0, 10.0, 100.0 and 1000.0, the goal being to compare the implementations with various time steps.

A parameter pair is then considered successful if the solver was able to both reach a residual norm lower than the minimum value reached without SFD and reach a lift coefficient value with a difference with the theoretical value of 0 that is lower than 0.01. The reasoning for

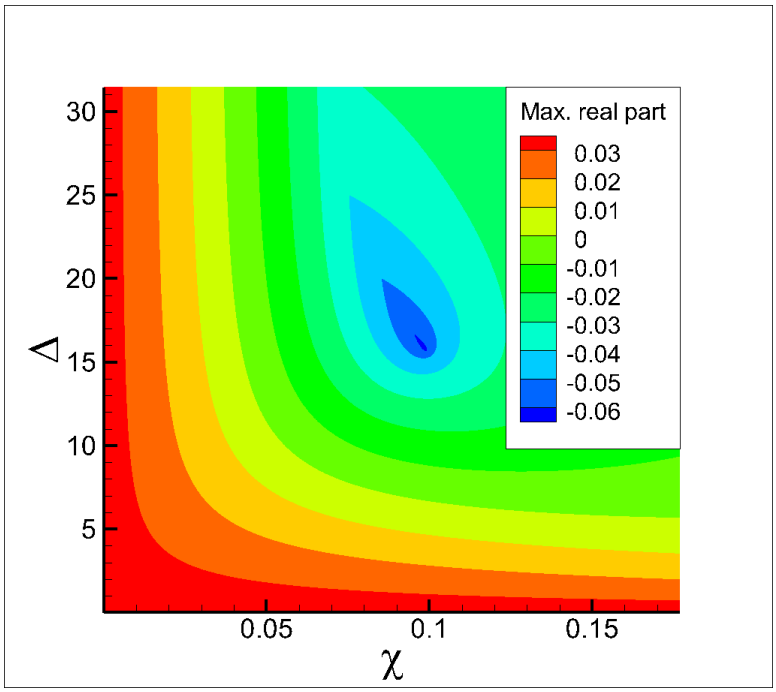

Figure 4.13 Maximum real part of the two modified eigenvalues computed during the final optimization of the χ and Δ parameters

this methodology is that for a parameter pair to be useful in practice, it must both allow the solver to converge and to reach valid values of the aerodynamic coefficients in an acceptable amount of iterations.

The successful parameters for the different cases are displayed in Fig.4.15, 4.17, 4.19 and 4.21 where they are identified with "o" marks, while the unsuccessful parameters are identified with "x" marks. For low CFL numbers of 5.0 and 10.0, it can be seen that the coupled formulation displayed more successful parameter pairs and that all the successful parameter pairs displayed by the encapsulated formulation are shared with the coupled formulation. However, when large CFL numbers such as 100.0 and 1000.0 are used the successful parameters are different for each formulation. This result agrees with the expectation that a large time step would cause the behavior of the two formulations to differ. The limitations of the analysis presented in Sec.3.2.4 is also observed since the successful parameters for the coupled formulation vary when the CFL number is increased, with the parameters found with the theoretical 1-D model being suitable at low CFL number but becoming unsuitable at high CFL numbers. This behavior that is not predicted by the simplified 1-D model is not surprising either, since it can be expected that when a large time step is used the numerical effects coming from the temporal and spatial schemes can no longer be neglected to solely

focus on the physical phenomenon.

From these results it is concluded that special care must be taken to avoid using a time step that would be too large with the adaptive SFD algorithm, since the numerical effects could make the parameter selection analysis insufficient. This limitation of the algorithm could potentially be improved in future works.

4.2 Buffet over transonic airfoil

4.2.1 OAT15A testcase

The ESFD with the filter reset is now tested for a case with turbulence modeling. The selected case is the OAT15A airfoil at an angle of attack of 3.5 degrees, Mach number of 0.73 and Reynolds number of 3 million. In these flow conditions the transonic buffet phenomenon is observed [60]. The turbulence model is the Spalart-Allmaras model with Edwards-Chandra modification and compressibility correction [53] [54]. For all the simulations in this section the CFL number is set to 5.5 and 3 grid levels are used in the W-cycle multigrid algorithm. The mesh consists of a structured O-grid. The chord of the profile is set to 1.0 and the farfield is placed at 50 chords of the profile.

This test case is particularly used to conduct parametric studies of the effect of the choice of parameters in the ESFD implementation of NSCODE, which are presented in the following subsections.

Delta\Chi	0.001	0.01	0.1	1.0	10.0	100.0	1000.0
0.001	x	x	x	x	x	o	o
0.01	x	x	x	x	o	o	x
0.1	x	x	x	o	o	x	x
1.0	x	x	o	o	x	x	x
10.0	x	o	o	o	x	x	x
100.0	o	o	o	x	x	x	x
1000.0	o	o	x	x	x	x	x

Successful parameter pairs identified with a "o" mark with the coupled formulation

Delta\Chi	0.001	0.01	0.1	1.0	10.0	100.0	1000.0
0.001	x	x	x	x	x	x	x
0.01	x	x	x	x	x	x	x
0.1	x	x	x	x	x	x	x
1.0	x	x	o	o	x	x	x
10.0	x	o	o	o	x	x	x
100.0	o	o	o	x	x	x	x
1000.0	o	o	x	x	x	x	x

Successful parameter pairs identified with a "o" mark with the encapsulated formulation

Figure 4.15 Comparison of the successful parameter pairs on the laminar flow over cylinder case in CHAMPS for different SFD formulations, CFL=5.0

Delta\Chi	0.001	0.01	0.1	1.0	10.0	100.0	1000.0
0.001	x	x	x	x	x	x	x
0.01	x	x	x	x	x	x	x
0.1	x	x	x	x	x	x	x
1.0	x	x	x	x	x	x	x
10.0	x	x	o	o	x	x	x
100.0	x	o	o	o	x	x	x
1000.0	x	o	o	x	x	x	x

Successful parameter pairs identified with a "o" mark with the coupled formulation

Delta\Chi	0.001	0.01	0.1	1.0	10.0	100.0	1000.0
0.001	x	x	x	x	x	x	x
0.01	x	x	x	x	x	x	x
0.1	x	x	x	x	x	x	x
1.0	x	x	x	x	x	x	x
10.0	x	x	o	o	x	x	x
100.0	x	o	o	o	x	x	x
1000.0	x	o	o	x	x	x	x

Successful parameter pairs identified with a "o" mark with the encapsulated formulation

Figure 4.17 Comparison of the successful parameter pairs on the laminar flow over cylinder case in CHAMPS for different SFD formulations, CFL=10.0

Delta\Chi	0.001	0.01	0.1	1.0	10.0	100.0	1000.0
0.001	x	x	x	x	x	x	x
0.01	x	x	x	x	x	x	x
0.1	x	x	x	x	x	x	x
1.0	x	x	x	x	x	x	x
10.0	x	x	x	x	x	x	x
100.0	x	x	o	o	x	x	x
1000.0	x	x	o	o	x	x	x

Successful parameter pairs identified with a "o" mark with the coupled formulation

Delta\Chi	0.001	0.01	0.1	1.0	10.0	100.0	1000.0
0.001	x	x	x	x	x	x	x
0.01	x	x	x	x	x	x	x
0.1	x	x	x	x	x	x	x
1.0	x	x	x	x	x	x	x
10.0	x	x	x	x	x	x	x
100.0	x	o	o	x	x	x	x
1000.0	x	o	x	x	x	x	x

Successful parameter pairs identified with a "o" mark with the encapsulated formulation

Figure 4.19 Comparison of the successful parameter pairs on the laminar flow over cylinder case in CHAMPS for different SFD formulations, CFL=100.0

Delta\Chi	0.001	0.01	0.1	1.0	10.0	100.0	1000.0
0.001	x	x	x	x	x	x	x
0.01	x	x	x	x	x	x	x
0.1	x	x	x	x	x	x	x
1.0	x	x	x	x	x	x	x
10.0	x	x	x	x	x	x	x
100.0	x	x	x	x	x	x	x
1000.0	x	x	o	o	x	x	x

Successful parameter pairs identified with a "o" mark with the coupled formulation

Delta\Chi	0.001	0.01	0.1	1.0	10.0	100.0	1000.0
0.001	x	x	x	x	x	x	x
0.01	x	x	x	x	x	x	x
0.1	x	x	x	x	x	x	x
1.0	x	x	x	x	x	x	x
10.0	x	x	x	x	x	x	x
100.0	x	x	x	x	x	x	x
1000.0	o	o	x	x	x	x	x

Successful parameter pairs identified with a "o" mark with the encapsulated formulation

Figure 4.21 Comparison of the successful parameter pairs on the laminar flow over cylinder case in CHAMPS for different SFD formulations, CFL=1000.0

4.2.2 Parametric sweep of χ and Δ

To observe the sensitivity of the solver to the χ and Δ parameters used, a parametric sweep is conducted for these two parameters on the initially unconverging case. This first sweep is conducted without any periodic reset of the filtered flow. The methodology for this test is to let the solver run for 100 000 iterations while only varying the χ and Δ parameters of the case.

A pair of parameters can results in the solver not being able to converge to a steady solution, either because the choice of parameters causes the solver to diverge from a steady solution until it encounters an error because of an out of bound value or because it results in the solver being unable to damp the unsteady phenomenon and to display a limit-cycle oscillation in the residual convergence that prevents it from converging further. The appearance of one of these conditions determines the lower boundaries of the considered χ and Δ parameters. The upper boundary of both parameters is arbitrary and is chosen because the trend observed is that the convergence rate of the solver is degrading as one parameter increases when the other is maintained at a constant value.

For the parameters pairs that are able to stabilize the oscillations, the logarithm of the root mean square value of the density residual, normalized by the value before the first iteration, is used as the criterion to determine the best convergence rate that can be obtained. The results are displayed in Fig. 4.22. The parameters couple resulting in the lowest convergence and as such the best convergence rate is $\chi = 4.0$ and $\Delta = 0.05$.

A more detailed observation of the residual convergence evolution with the solver iterations for these stabilized runs shows that the convergence rate seems to decrease after a certain point, where a convergence stalling behavior appears. This can be seen in Fig. 4.23 for the identified optimal parameters pair and two other parameters pairs arbitrarily chosen to illustrate the general behavior observed. In the case of the optimal parameters pair, this stalling behavior seems to appear at approximately 25 000 iterations.

4.2.3 Parametric sweep of reset period with constant χ and Δ

After an optimal parameter pair of $\chi = 4.0$ and $\Delta = 0.05$ is identified, the effects of the periodic reset are investigated by conducting a second parametric sweep on the period of the periodic reset. The optimal parameters identified without reset are used during this sweep. The stopping criterion for a simulation in this test is either to reach 100 000 iterations or

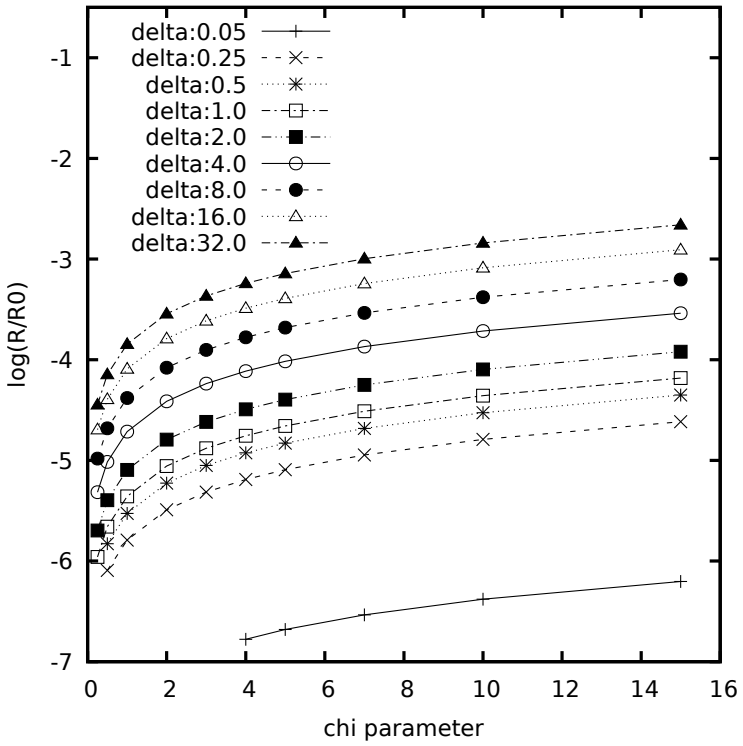

Figure 4.22 Parametric study of residual convergence after 100 000 iterations of solver for various SFD parameters pairs

to reach a level of convergence of 7 orders of magnitude. This is because in the parametric sweep without any reset, which was also limited to 100 000 iterations, no parameter pairs allowed the solver to reach a better convergence than 7 orders of magnitude. The results, shown in Fig. 4.24 with the original case without reset provided for comparison purpose, are that while an unsuitable parameter for the reset period prevents the solver from converging, a suitable parameter value does mitigate the convergence stalling behavior observed in the initial case without reset. In this case the best result for a reset period value is a period of 10 000 iterations, which results in the 7.0 order of convergence criterion to be reached in 41 434 iterations.

4.2.4 Parametric sweep of χ, Δ and reset period

A parametric sweep of the reset period for constant χ and Δ parameters is useful to isolate the effect of the reset parameter. However, based on the fact that the original goal of the reset of the filtered flow is to counteract the convergence stalling behavior when SFD is applied and that this convergence stalling can vary with the choice of χ and Δ parameters,

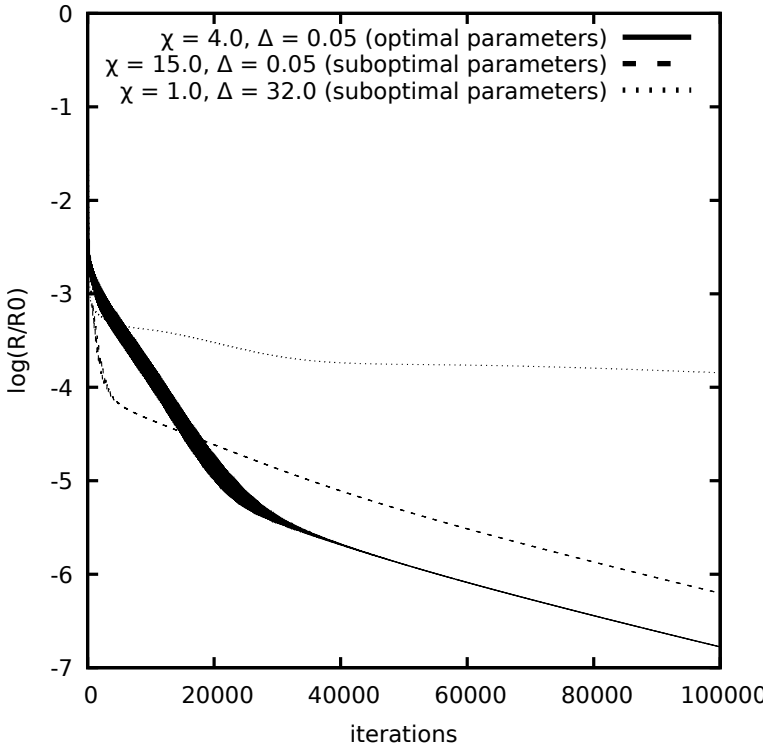

Figure 4.23 Residual convergence of buffet over the OAT15A airfoil case with ESFD for a RANS simulation

studying the effect of the reset period when the other parameters are not kept constant is also of interest. For this reason, a parametric sweep is conducted simultaneously on the three parameters to further study their interaction.

The results are displayed in Fig. 4.26. For all displayed parameter combinations the solver reaches the criterion of 7 orders of magnitude of residual convergence. This is a better convergence level than what is achieved in 100 000 iterations in the best case of the parametric sweep without any reset. The number of iterations necessary to reach this residual convergence level is significantly lower compared to the case without reset, being approximately 3500 iterations in the best cases. Several parameter triplets reach this approximate value. This represents a reduction of solver iterations of roughly 96.5 percent to reach a better residual convergence level than what is achieved without reset, a clear improvement in terms of computational cost. The results also highlight the fact that the value of the optimal parameters of the SFD method changes when a periodic reset is added to the method.

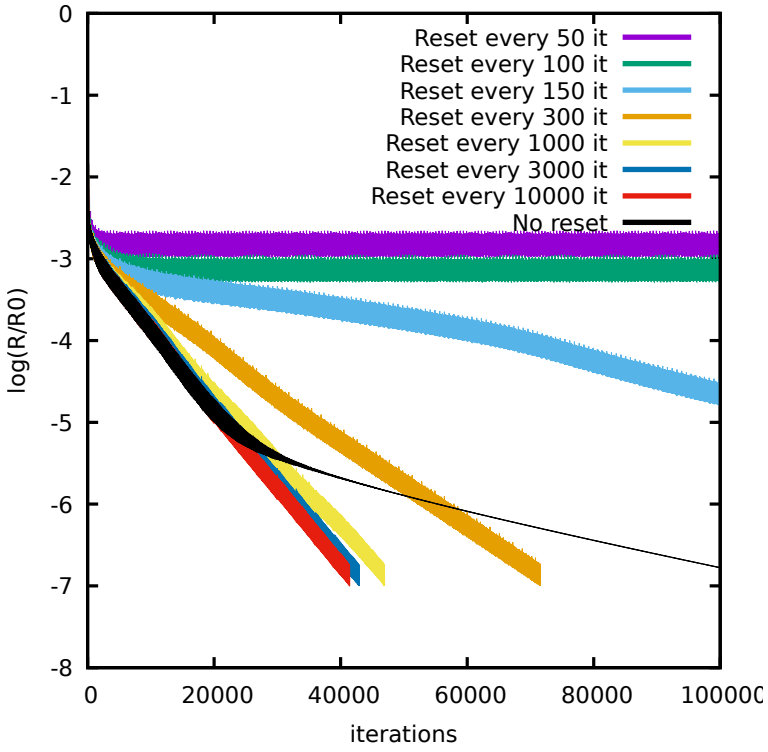

Figure 4.24 Parametric study of reset period for a constant SFD parameters pair

A phenomenon also observed is that as expected some selections of parameters are less optimal than others when considering convergence rate and that not all triplets of parameters are able to make the solver converge. It is noted however that even for sub-optimal parameters displayed in Fig. 4.26 the number of iterations required to reach the convergence criterion is significantly lower than in the case without reset or the reset period parametric sweep with constant χ and Δ parameters. The addition of a periodic reset to the numerical scheme can as such be a positive addition for the solver even if sub-optimal parameters are selected.

To confirm the fact that the solution reached with such a major increase in convergence rate is still a valid solution, the variation of the lift coefficient along the solver iterations is provided in Fig. 4.27. The evolution of the lift coefficient for the solver using SFD with and without a periodic reset of the filtered flow is provided alongside a line indicating the value of the lift coefficient of the flow solution when machine accuracy is reached. It is possible to see that in both cases the solver converges toward the machine accurate solution, albeit at a much slower rate in the case without a periodic reset.

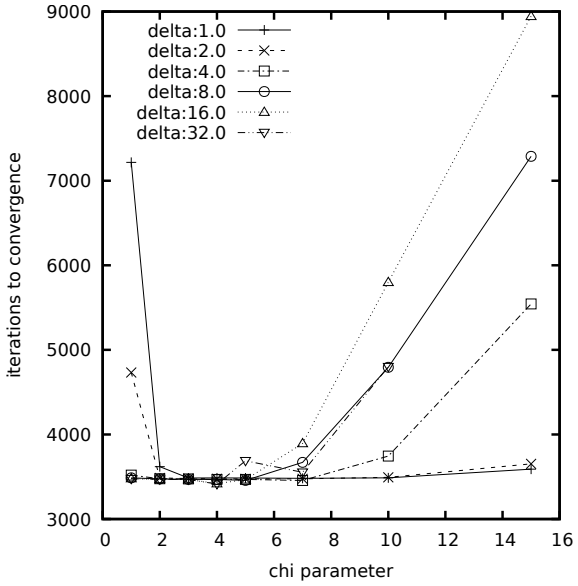

Required iterations to reach 7 orders of residual convergence for various SFD parameters and a reset period of 50 iterations in NSCODE

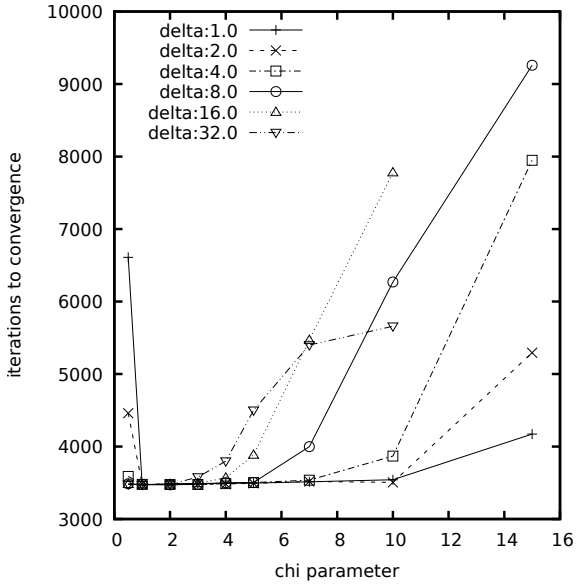

Required iterations to reach 7 orders of residual convergence for various SFD parameters and a reset period of 100 iterations in NSCODE

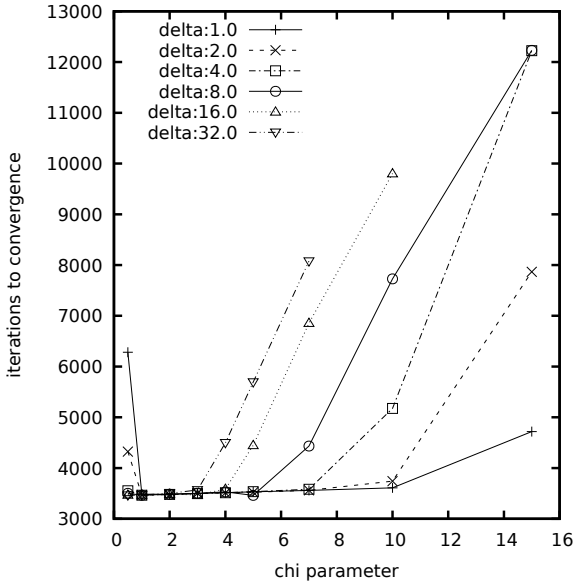

Required iterations to reach 7 orders of residual convergence for various SFD parameters and a reset period of 150 iterations in NSCODE

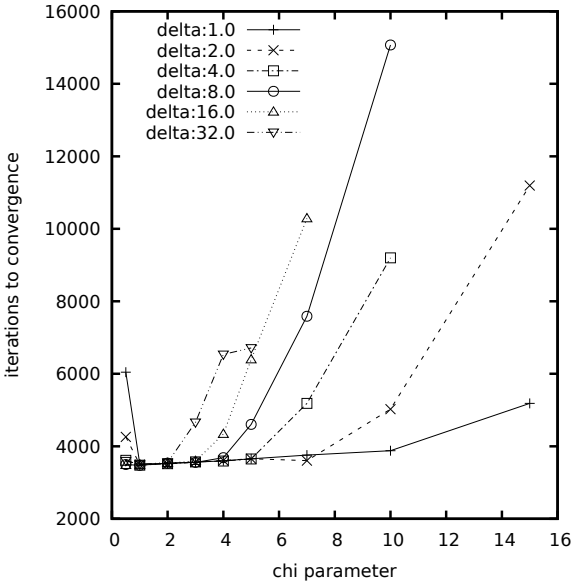

Required iterations to reach 7 orders of residual convergence for various SFD parameters and a reset period of 300 iterations in NSCODE

Figure 4.26 Parametric study of SFD parameters triplets

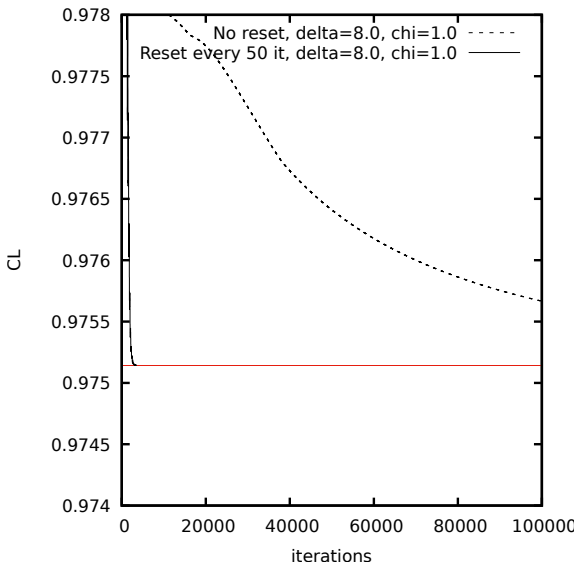

Figure 4.27 Comparison of lift coefficient of the transonic OAT15A case for a RANS simulation stabilized with SFD, with and without periodic reset

4.3 Multi element airfoil in stall conditions

To demonstrate the capabilities of the SFD implementations to stabilize an unstable phenomenon on a complex case, the case of a vortex shedding in the wake of a 3-element airfoil in stall conditions is studied. The specific case used is the 2-D multi elements airfoil section of the High-Lift Common Research Model shown in Fig. 4.28, available in the turbulence modeling resource database of NASA [61]. The flow conditions for this test are a Mach number of 0.2 and a Reynolds number of 5 million. The turbulence model used is the Spalart-Allmaras model and an implicit SGS solver is used to advance the problem in time. The stopping criterion for the convergence of the cases is a reduction of 8 orders of magnitude of the norm of the density residual.

The test case is run using the CHAMPS solver, which is compatible with the unstructured meshes provided for this more complex geometry. Seven meshes are provided for this case, with an increasing amount of cells. The mesh used in this case contains 508366 cells and corresponds to the third mesh, selected as a compromise between accuracy and computational cost. Reference results are available in the literature for this test case, particularly for an angle of attack of 16 degrees. The case is first run at this angle of attack without using SFD to compare the result of the CHAMPS solver with the NASA reference values.

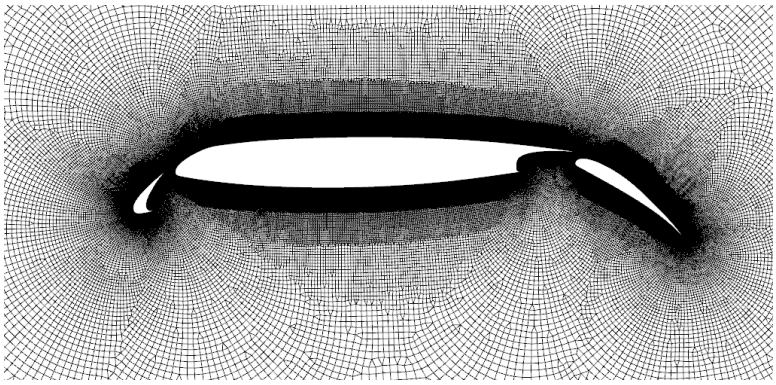

Figure 4.28 Zoomed view of the 2D High-Lift CRM wing section unstructured mesh

The location of re-circulation zones and the stagnation point location, shown in Fig. 4.29, are in agreement with the flow field presented in an identical test case from the literature [62]. The aerodynamics coefficients obtained with the FUN3D solver show an important variation between the coarsest mesh and the finest mesh because of mesh while achieving grid convergence. The lift coefficient obtained by FUN3D varies from 3.57 for the coarsest mesh to 3.78 for the finest mesh. The drag coefficient varies from 0.076 for the coarsest mesh to 0.062 for the finest mesh. The values obtained with CHAMPS for the lift and drag coefficient values are respectively 3.59 and 0.076. While the values obtained have a difference with the grid converged reference values that is not negligible, the results are considered acceptable for the purpose of testing the stabilization method. The reason for this is that they are inside the range of values obtained in the reference case on the coarser grids and that the CHAMPS test case uses a grid coarser than the one used to obtain the grid converged values in FUN3D.

The geometry with these flow conditions is then tested for a range of angles of attack to create the lift polar for this airfoil starting at 0.0 by an increment of 1.0. The initial condition for each angle of attack simulation is the converged solution of the previous angle of attack simulation. No instability is observed up to the post-stall angle of attack of 28.0 where the flow is not fully separated over the main element of the airfoil, as shown in Fig. 4.30a. At the angle of attack 29.0, the flow becomes fully separated over the main element of the airfoil as shown in Fig. 4.30b which causes a sudden drop in lift coefficient. It can be observed in Fig. 4.32 that the rate of convergence of the solver is reduced as this angle of attack is approached and that the sum of the residual even initially rises before the solver converges to a flow field fully separated from the main element at the angle of attack of 29.0.

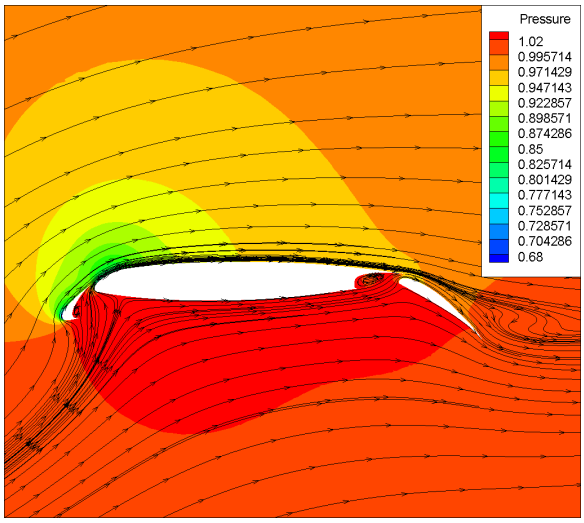

Figure 4.29 Streamlines and pressure around the 2D High-Lift CRM wing section unstructured mesh at α=16.0

When the simulations for angles of attack after 29.0 degrees are performed using the converged flow fully detached from the main element as an initial condition, the subsequent converged solutions also present the same separation. However, by using a flow field that is not fully detached from the main element as the initial condition for the next angle of attack of 30.0, another converged flow can be obtained where the flow is not fully separated. This solution consequently has a higher lift coefficient. The flow fields of these two solutions are shown in Fig. 4.34. This multiplicity of solutions at the same angle of attack for an airfoil in stall conditions is a known phenomenon that can be found in the literature [22] [23] [11] for simpler single element airfoils. Solutions for subsequent angles of attack can be obtained by using either flows as an initial condition to continue the polar, resulting in two different new solutions. These solutions can in turn be used as an initial condition to evaluate other subsequent angles of attack resulting from these two initial conditions.

These multiple solutions will be referred to as two branches of solutions. The solutions originating from the use of the converged flow field with a full separation over the main element of the airfoil at α=30.0 will be referred to as the first branch of solutions. The solutions originating from the use of the flow field that is not fully separated from the main element at α=30.0 will be referred to as the stabilized branch since some solutions of this branch will require stabilization through the use of SFD. Both branches are continued up to an angle of attack of 34.0 degrees.

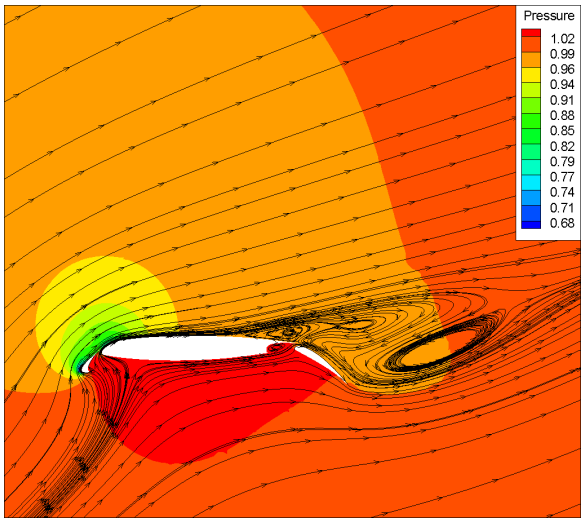

Streamlines and pressure around the 2D High-Lift CRM wing section unstructured mesh at α=28.0

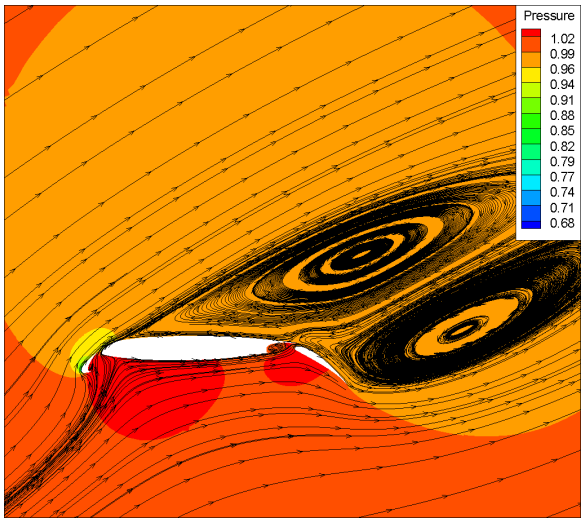

Streamlines and pressure around the 2D High-Lift CRM wing section unstructured mesh at α=29.0

Figure 4.31 Comparison of streamlines and pressure around the 2D High-Lift CRM wing section before and after full separation of the flow over the main element of the airfoil

When computing the angles of attack of the stabilized branch, instabilities that prevent the solver from converging are encountered at angles of attack of 31.0, 32.0 and 34.0. Each of these angles of attack displays a different unsteady behavior, with varying lift coefficient amplitudes and frequencies respective to iterations. The coupled SFD implementation in CHAMPS is used to stabilize the flow at the 31.0 and 34.0 angles of attack. The suitable SFD parameters for these cases are found with a basic parametric study for each angle, limited in scope by the computational cost of running the simulation repeatedly. The parameters selected for the angle of attack of 31.0 are a χ,Δ and reset period values of 0.5, 50.0 and 20000 respectively. For the angle of attack of 34.0, these parameters have values of 0.1, 10.0 and 5000. No suitable parameters were found to stabilize the instability at the angle of attack of 32.0 with this limited methodology, which highlights the importance of a reliable parameter selection method. The lift coefficient values of the converged flow fields in this stabilized branch are displayed in Fig. 4.35 along with the other lift coefficients obtained for this polar.

The main difference observed between the solutions of the stabilized branch and the solutions of the first branch is the area of the airfoil over which the flow is separated. In particular, at an angle of attack of 34.0, the main difference between the two flow fields seems to be a separation of the flow over the slat of the airfoil in the stabilized branch. These fields can be observed in Fig. 4.37 and Fig. 4.39.

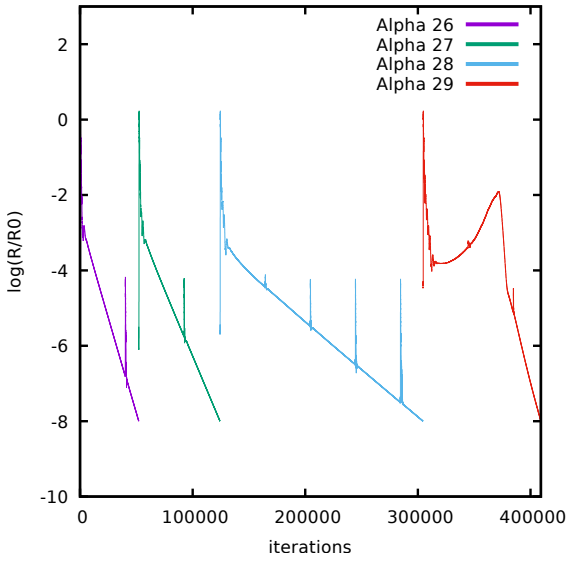

Figure 4.32 Residual convergence for angles of attack before and during the occurrence of the complete separation of the flow for the 2D High-Lift CRM case

The stabilization of these angle of attacks highlights the capability of the implemented SFD stabilization with a local time-stepping scheme to be used on complex industrially relevant cases and to study the phenomenon of multiple solutions in subsonic stall conditions on these geometries, as done by Richez et al. [22] and Plante et al. [23] on the simpler geometry of a single element airfoil.

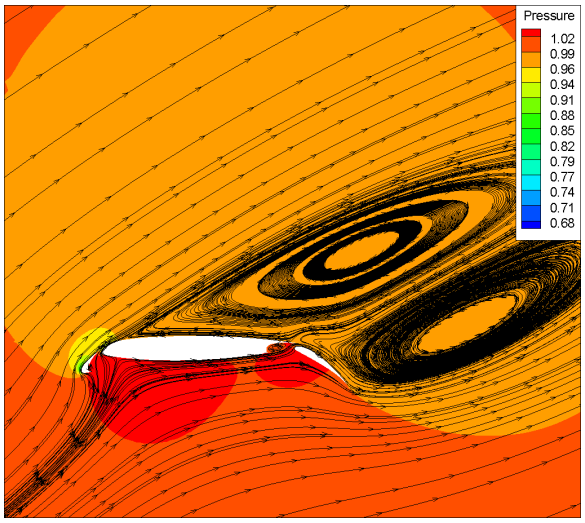

Streamlines and pressure around the 2D High-Lift CRM wing section unstructured mesh at α=30.0, first branch

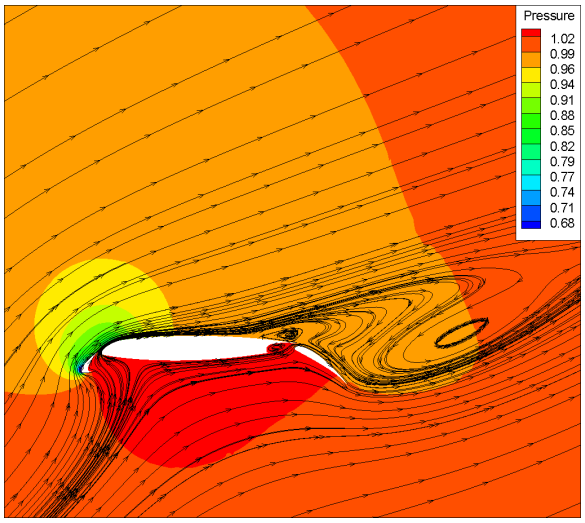

Streamlines and pressure around the 2D High-Lift CRM wing section unstructured mesh at α=30.0, stabilized branch

Figure 4.34 Comparison of streamlines and pressure around the 2D High-Lift CRM wing section for the first branch and stabilized branch at α=30.0

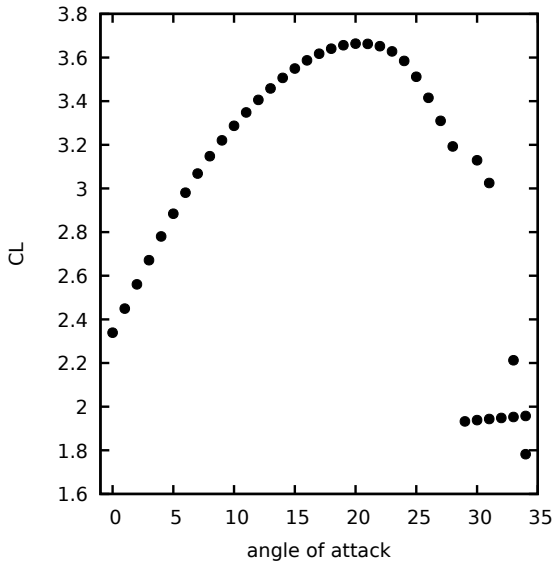

Figure 4.35 Lift coefficient for various angle of attacks obtained for the 2D High-Lift CRM case

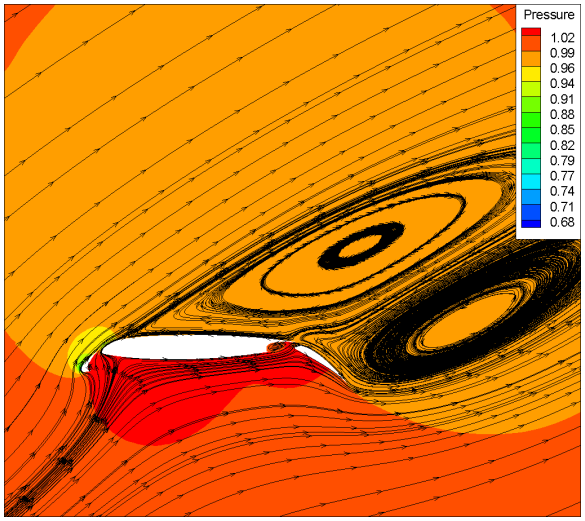

Streamlines and pressure around the 2D High-Lift CRM wing section unstructured mesh at α=31.0, first branch

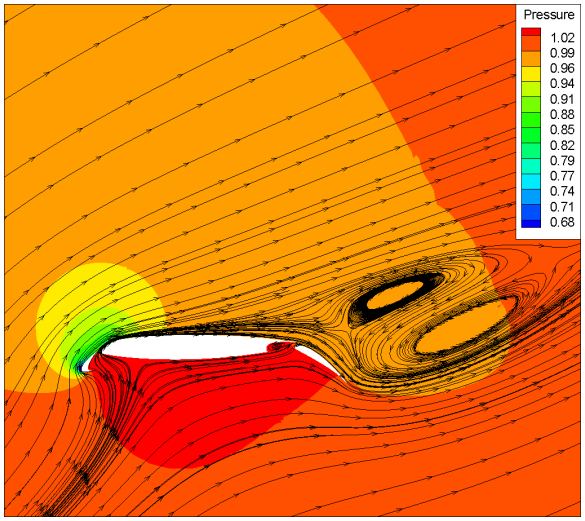

Streamlines and pressure around the 2D High-Lift CRM wing section unstructured mesh at α=31.0, stabilized branch

Figure 4.37 Comparison of streamlines and pressure around the 2D High-Lift CRM wing section for the first branch and stabilized branch at α=31.0

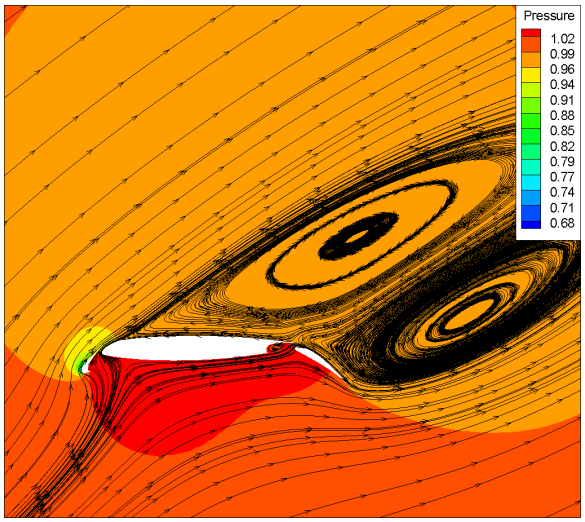

Streamlines and pressure around the 2D High-Lift CRM wing section unstructured mesh at α=34.0, first branch

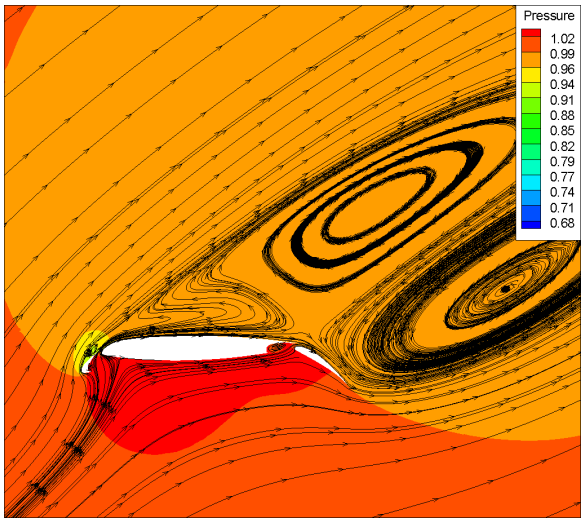

Streamlines and pressure around the 2D High-Lift CRM wing section unstructured mesh at α=34.0, stabilized branch

Figure 4.39 Comparison of streamlines and pressure around the 2D High-Lift CRM wing section for the first branch and stabilized branch at α=34.0

CHAPTER 5 CONCLUSION

5.1 Summary of works

The main objective of this work is to develop, implement, verify and validate an algorithm able to damp oscillations preventing a RANS solver from converging toward a steady solution. To achieve this goal an algorithm using the Selective Frequency Damping method was developed and implemented in the NSCODE solver. In addition, an implementation of two formulations of the SFD method was performed in the CHAMPS solvers.

The first sub-objective was to compare the various SFD implementations presented in the literature. Two main formulations for SFD emerged, namely the original and encapsulated formulations. These formulations were compared with an analytical development on a simplified 1-D problem approximating a flow field dominated by a single eigenvalue. The analysis considers that an exact solver is used to advance the problem in time. The main result from the analysis is that while the two formulations are equivalent on a smaller time step, their behavior may differ when using a large time step. Another prediction from this analysis is that the encapsulated formulation should lose its efficiency and be unable to damp unstable modes when the time step becomes large.

The two formulations were subsequently implemented in the 3D unstructured CHAMPS solver. Their behavior was compared on the test case of vortex shedding in the wake of a cylinder in a laminar flow. The results obtained confirm the expected difference between the two formulations when using a large time step. However, the expectation that the encapsulated formulation should be unable to stabilize an unstable flow when a large time step is not validated, indicating that the simplified analysis is useful but has limitations.

The second sub-objective was to investigate potential improvements of the existing SFD stabilization implementations. The most important improvement made to the method in the implementation of this work is the addition of a periodic reset of the filtered flow field to the value of the physical flow field. This new step in the algorithm is added to improve the convergence rate by removing the convergence stalling behavior observed on various test cases. The effect of this additional step is observed through a parametric sweep of the χ, Δ and reset period parameters. The results of the tests indicate that a suitable choice of periodic reset is able to improve the convergence rate of the solver when using SFD.

In addition to the periodic reset, other improvements were made on the adaptive SFD algorithm implemented in NSCODE compared with the original implementation presented by Jordi et al. [44]. The first one is the fact that the algorithm is used in a local time-stepping scheme. The second one is the use of the analytical model based on the original coupled SFD formulation to compute the modification of the dominant eigenvalue instead of the encapsulated formulation, which diminishes the computational cost of the algorithm. The adaptive algorithm, including the global stability analysis, the optimization of the eigenvalues and the stabilization through the use of SFD is used on the test case of vortex shedding over a cylinder with satisfactory results.

The functionality of the original coupled formulation of SFD implemented in CHAMPS is also demonstrated on a more complex case of a 3-elements airfoil in stall conditions to show the potential of stabilization on industrially relevant cases with various instabilities. In doing so, it also extended results obtained on single element airfoils to a 3-elements airfoil of the multiplicity of solutions at post-stall angles of attack. This hysteresis phenomenon is observed in the separation of the flow from the airfoil.

5.2 Limitations

The SFD method itself as a stabilization technique has limitations. Since it uses a low-pass filter to remove oscillations, SFD is not able to stabilize unsteady cases that are not oscillating. In addition to this, the analysis done in this work to choose suitable SFD parameters also has limitations. The first one is the assumption that only one unstable frequency is present in a test case. The second is the approximation of the evolution of the flow being represented by an exact solver. This removes the effect of the temporal and spatial schemes of the solver in the analysis. It was however shown by Plante & Laurendeau [42] that the oscillations influenced by these numerical schemes can be damped by SFD.

The assumption of a "frozen" turbulent viscosity variable in the SFD implementations and the global stability analysis being implemented only for laminar flow equations is also a limitation of this work.

Even though the adaptive SFD algorithm was implemented in NSCODE and the coupled SFD implementation of CHAMPS was tested on a 3-element airfoil case, the adaptive algorithm was not implemented in the 3-D unstructured solver CHAMPS. This resulted in the adaptive algorithm not being tested on more complex cases such as the 3-elements airfoil.

Finally, the additional periodic reset added to improve the convergence rate is limited in its implementation by the fact that the methodology used to set the value of its period in this work is based on manual setting and observation.

5.3 Future research

Considering the limitations previously mentioned, possible future developments include the implementation of a similar adaptive SFD algorithm in the CHAMPS solver to consider more complex cases. The SFD implementations could be extended to directly stabilize the turbulent viscosity variable in the case of turbulent flows. The global stability analysis implementation could be extended to include the turbulent viscosity variable and a sensitivity study could be conducted on the perturbation value ϵ for the computation of the jacobian matrix. The analysis of the effect of SFD on an unsteady eigenvalue could be extended by including the effect of the temporal and spatial scheme to replace the approximation of an exact solver. Finally, the selection of the period for the reset of the low-pass time-filtered flow can be improved. A possible method would be to include this reset in the analysis of the effect of SFD by identifying which eigenvalue is most related to the evolution of the time-filtered flow by computing the corresponding modified eigenvector of the two modified eigenvalues. These developments could also allow to expand the scope of the current work and optimize the choice of the parameters of SFD to accelerate the convergence rate of a solver, an application that was shown possible by Plante & Laurendeau [42] but for which an analytical parameter selection methodology is not yet present in the literature.

REFERENCES

[1] E. N. Tinoco, D. R. Bogue, T.-J. Kao, N. J. Yu, P. Li, and D. N. Ball, "Progress toward CFD for full flight envelope," *The Aeronautical Journal*, vol. 109, no. 1100, pp. 451–460, Oct. 2005, publisher: Cambridge University Press. [Online]. Available: https://doi.org/10.1017/S0001924000000865

[2] J. D. Crouch, A. Garbaruk, and D. Magidov, "Predicting the onset of flow unsteadiness based on global instability," *Journal of Computational Physics*, vol. 224, no. 2, pp. 924–940, Jun. 2007. [Online]. Available: https://doi.org/10.1016/j.jcp.2006.10.035

[3] J. Blazek, *Computational Fluid Dynamics : Principles and Applications*, 1st ed. Oxford, UK: Elsevier, 2001.

[4] P. Spalart and S. Allmaras, "A one-equation turbulence model for aerodynamic flows," in *30th Aerospace Sciences Meeting and Exhibit*, ser. Aerospace Sciences Meetings. American Institute of Aeronautics and Astronautics, Jan. 1992. [Online]. Available: https://doi.org/10.2514/6.1992-439

[5] A. Jameson, "Time dependent calculations using multigrid, with applications to unsteady flows past airfoils and wings," in *10th Computational Fluid Dynamics Conference*, ser. Fluid Dynamics and Co-located Conferences. American Institute of Aeronautics and Astronautics, Jun. 1991. [Online]. Available: https://doi.org/10.2514/6.1991-1596

[6] B. N. Rajani, A. Kandasamy, and S. Majumdar, "Numerical simulation of laminar flow past a circular cylinder," *Applied Mathematical Modelling*, vol. 33, no. 3, pp. 1228–1247, Mar. 2009. [Online]. Available: https://doi.org/10.1016/j.apm.2008.01.017

[7] S. Yarusevych, P. E. Sullivan, and J. G. Kawall, "On vortex shedding from an airfoil in low-Reynolds-number flows," *Journal of Fluid Mechanics*, vol. 632, pp. 245–271, Aug. 2009, publisher: Cambridge University Press. [Online]. Available: https://doi.org/10.1017/S0022112009007058

[8] O. O. Bendiksen, "Review of unsteady transonic aerodynamics: Theory and applications," *Progress in Aerospace Sciences*, vol. 47, no. 2, pp. 135–167, Feb. 2011. [Online]. Available: https://doi.org/10.1016/j.paerosci.2010.07.001

[9] F. Plante, J. Dandois, S. Beneddine, D. Sipp, and E. Laurendeau, "Numerical simulations and global stability analyses of transonic buffet and subsonic stall," in *AAAF AERO2019*, PARIS, France, Mar. 2019. [Online]. Available: https://hal.archives-ouvertes.fr/hal-02127307

[10] D. S. Kamenetskiy, J. E. Bussoletti, C. L. Hilmes, V. Venkatakrishnan, L. B. Wigton, and F. T. Johnson, "Numerical Evidence of Multiple Solutions for the Reynolds-Averaged Navier–Stokes Equations," *AIAA Journal*, vol. 52, no. 8, pp. 1686–1698, 2014. [Online]. Available: https://doi.org/10.2514/1.J052676

[11] D. Busquet, O. Marquet, F. Richez, M. Juniper, and D. Sipp, "Global stability analysis of turbulent flows around an airfoil near stall," in *EUROGEN 2017*, Madrid, Spain, Sep. 2017. [Online]. Available: https://www.researchgate.net/publication/319746431_Global_stability_analysis_of_turbulent_flows_around_an_airfoil_near_stall

[12] C. Wales, A. L. Gaitonde, D. P. Jones, D. Avitabile, and A. R. Champneys, "Numerical continuation of high Reynolds number external flows," *International Journal for Numerical Methods in Fluids*, vol. 68, no. 2, pp. 135–159, 2012. [Online]. Available: https://doi.org/10.1002/fld.2497

[13] M. M. Zdravkovich, *Flow Around Circular Cylinders: A Comprehensive Guide through Flow Phenomena, Experiments, Applications, Mathematical Models, and Computer Simulations*. Oxford, New York: Oxford University Press, Jul. 1997, vol. 1.

[14] C. H. K. Williamson, "Defining a universal and continuous Strouhal–Reynolds number relationship for the laminar vortex shedding of a circular cylinder," *The Physics of Fluids*, vol. 31, no. 10, pp. 2742–2744, Oct. 1988, publisher: American Institute of Physics. [Online]. Available: https://doi.org/10.1063/1.866978

[15] A. Gopinath and A. Jameson, "Application of the Time Spectral Method to Periodic Unsteady Vortex Shedding," in *44th AIAA Aerospace Sciences Meeting and Exhibit*, ser. Aerospace Sciences Meetings. American Institute of Aeronautics and Astronautics, Jan. 2006. [Online]. Available: https://doi.org/10.2514/6.2006-449

[16] A. Mosahebi and S. Nadarajah, "An Adaptive Nonlinear Frequency Domain Method for Viscous Periodic Steady State Flows," in *48th AIAA Aerospace Sciences Meeting Including the New Horizons Forum and Aerospace Exposition*, ser. Aerospace Sciences Meetings. American Institute of Aeronautics and Astronautics, Jan. 2010. [Online]. Available: https://doi.org/10.2514/6.2010-1267

[17] L. Jacquin, P. Molton, S. Deck, B. Maury, and D. Soulevant, "Experimental Study of Shock Oscillation over a Transonic Supercritical Profile," *AIAA Journal*, vol. 47, no. 9, pp. 1985–1994, Sep. 2009, publisher: American Institute of Aeronautics and Astronautics. [Online]. Available: https://doi.org/10.2514/1.30190

[18] F. Grossi, M. Braza, and Y. Hoarau, "Prediction of Transonic Buffet by Delayed Detached-Eddy Simulation," *AIAA Journal*, vol. 52, no. 10, pp. 2300–2312, Apr. 2014, publisher: American Institute of Aeronautics and Astronautics. [Online]. Available: https://doi.org/10.2514/1.J052873

[19] F. Sartor, C. Mettot, and D. Sipp, "Stability, Receptivity, and Sensitivity Analyses of Buffeting Transonic Flow over a Profile," *AIAA Journal*, vol. 53, no. 7, pp. 1980–1993, Dec. 2014, publisher: American Institute of Aeronautics and Astronautics. [Online]. Available: https://doi.org/10.2514/1.J053588

[20] J. A. Hoffmann, "Effects of freestream turbulence on the performance characteristics of an airfoil," *AIAA Journal*, vol. 29, no. 9, pp. 1353–1354, Sep. 1991, publisher: American Institute of Aeronautics and Astronautics. [Online]. Available: https://doi.org/10.2514/3.10745

[21] G. Hristov and P. J. Ansell, "Post-Stall Hysteresis and Flow Field Unsteadiness on an NACA 0012 Airfoil," in *55th AIAA Aerospace Sciences Meeting*. American Institute of Aeronautics and Astronautics, Jan. 2017. [Online]. Available: https://doi.org/10.2514/6.2017-0997

[22] F. Richez, M. Leguille, and O. Marquet, "Selective frequency damping method for steady RANS solutions of turbulent separated flows around an airfoil at stall," *Computers & Fluids*, vol. 132, pp. 51–61, Jun. 2016. [Online]. Available: https://doi.org/10.1016/j.compfluid.2016.03.027

[23] F. Plante, J. Dandois, and E. Laurendeau, "Similarities Between Cellular Patterns Occurring in Transonic Buffet and Subsonic Stall," *AIAA Journal*, vol. 58, no. 1, pp. 71–84, 2020. [Online]. Available: https://doi.org/10.2514/1.J058555

[24] E. Akervik, L. Brandt, D. S. Henningson, J. Hœpffner, O. Marxen, and P. Schlatter, "Steady solutions of the Navier-Stokes equations by selective frequency damping," *Physics of Fluids*, vol. 18, no. 6, p. 068102, Jun. 2006, publisher: American Institute of Physics. [Online]. Available: https://doi.org/10.1063/1.2211705

[25] C. D. Pruett, B. C. Thomas, C. E. Grosch, and T. B. Gatski, "A temporal approximate deconvolution model for large-eddy simulation," *Physics of Fluids*, vol. 18, no. 2, p. 028104, Feb. 2006, publisher: American Institute of Physics. [Online]. Available: https://doi.org/10.1063/1.2173288

[26] C. D. Pruett, T. B. Gatski, C. E. Grosch, and W. D. Thacker, "The temporally filtered Navier–Stokes equations: Properties of the residual stress," *Physics of Fluids*, vol. 15, no. 8, pp. 2127–2140, Jun. 2003, publisher: American Institute of Physics. [Online]. Available: https://doi.org/10.1063/1.1582858

[27] P.-Y. Passaggia and U. Ehrenstein, "Optimal control of a separated boundary-layer flow over a bump," *Journal of Fluid Mechanics*, vol. 840, pp. 238–265, Apr. 2018, publisher: Cambridge University Press. [Online]. Available: https://doi.org/10.1017/jfm.2018.6

[28] S. Bagheri, P. Schlatter, P. J. Schmid, and D. S. Henningson, "Global stability of a jet in crossflow," *Journal of Fluid Mechanics*, vol. 624, pp. 33–44, Apr. 2009, publisher: Cambridge University Press. [Online]. Available: https://doi.org/10.1017/S0022112009006053

[29] M. Ilak, P. Schlatter, S. Bagheri, and D. S. Henningson, "Bifurcation and stability analysis of a jet in cross-flow: onset of global instability at a low velocity ratio," *Journal of Fluid Mechanics*, vol. 696, pp. 94–121, Apr. 2012, publisher: Cambridge University Press. [Online]. Available: https://doi.org/10.1017/jfm.2012.10

[30] J. W. Nichols and P. J. Schmid, "The effect of a lifted flame on the stability of round fuel jets," *Journal of Fluid Mechanics*, vol. 609, pp. 275–284, Aug. 2008, publisher: Cambridge University Press. [Online]. Available: https://doi.org/10.1017/S0022112008002528

[31] U. A. Qadri, G. J. Chandler, and M. P. Juniper, "Self-sustained hydrodynamic oscillations in lifted jet diffusion flames: origin and control," *Journal of Fluid Mechanics*, vol. 775, pp. 201–222, Jul. 2015, publisher: Cambridge University Press. [Online]. Available: https://doi.org/10.1017/jfm.2015.297

[32] B. Pier, "Local and global instabilities in the wake of a sphere," *Journal of Fluid Mechanics*, vol. 603, pp. 39–61, May 2008, publisher: Cambridge University Press. [Online]. Available: https://doi.org/10.1017/S0022112008000736

[33] B. Pier and N. Peake, "Global nonlinear dynamics of thin aerofoil wakes," in *Seventh IUTAM Symposium on Laminar-Turbulent Transition*, ser. IUTAM Bookseries, P. Schlatter and D. S. Henningson, Eds. Dordrecht: Springer Netherlands, 2010, pp. 319–324.

[34] P. Moise, "Bistability of bubble and conical forms of vortex breakdown in laminar swirling jets," *Journal of Fluid Mechanics*, vol. 889, Apr. 2020, publisher: Cambridge University Press. [Online]. Available: https://doi.org/10.1017/jfm.2020.105

[35] L. E. Jones and R. D. Sandberg, "Numerical analysis of tonal airfoil self-noise and acoustic feedback-loops," *Journal of Sound and Vibration*, vol. 330, no. 25, pp. 6137–6152, Dec. 2011. [Online]. Available: https://doi.org/10.1016/j.jsv.2011.07.009

[36] B. E. Jordi, C. J. Cotter, and S. J. Sherwin, "Encapsulated formulation of the selective frequency damping method," *Physics of Fluids*, vol. 26, no. 3, p. 034101, Mar. 2014, publisher: American Institute of Physics. [Online]. Available: https://doi.org/10.1063/1.4867482

[37] I. Farago, "Splitting Methods and Their Application to the Abstract Cauchy Problems," in *Numerical Analysis and Its Applications*, ser. Lecture Notes in Computer Science, Z. Li, L. Vulkov, and J. Waśniewski, Eds. Berlin, Heidelberg: Springer, 2005, pp. 35–45.

[38] J. Casacuberta, K. J. Groot, H. J. Tol, and S. Hickel, "Effectivity and efficiency of selective frequency damping for the computation of unstable steady-state solutions," *Journal of Computational Physics*, vol. 375, pp. 481–497, Dec. 2018. [Online]. Available: https://doi.org/10.1016/j.jcp.2018.08.056

[39] Y. Bengana, J.-C. Loiseau, J.-C. Robinet, and L. S. Tuckerman, "Bifurcation analysis and frequency prediction in shear-driven cavity flow," *Journal of Fluid Mechanics*, vol. 875, pp. 725–757, Sep. 2019, publisher: Cambridge University Press. [Online]. Available: https://doi.org/10.1017/jfm.2019.422

[40] A. Pini, A. Cammi, S. Lorenzi, M. T. Cauzzi, and L. Luzzi, "A CFD-based simulation tool for the stability analysis of natural circulation systems," *Progress in Nuclear Energy*, vol. 117, p. 103093, Nov. 2019. [Online]. Available: https://doi.org/10.1016/j.pnucene.2019.103093

[41] D. Rodriguez, E. M. Gennaro, and L. F. Souza, "Self-excited primary and secondary instability of laminar separation bubbles," *Journal of Fluid Mechanics*, vol. 906, Jan. 2021, publisher: Cambridge University Press. [Online]. Available: https://doi.org/10.1017/jfm.2020.767

[42] F. Plante and E. Laurendeau, "Acceleration of Euler and RANS solvers via Selective Frequency Damping," *Computers & Fluids*, vol. 166, pp. 46–56, Apr. 2018. [Online]. Available: https://doi.org/10.1016/j.compfluid.2018.01.027

[43] E. Paladini, O. Marquet, D. Sipp, J.-C. Robinet, and J. Dandois, "Various approaches to determine active regions in an unstable global mode: application to transonic buffet," *Journal of Fluid Mechanics*, vol. 881, pp. 617–647, Dec. 2019, publisher: Cambridge University Press. [Online]. Available: https://doi.org/10.1017/jfm.2019.761

[44] B. E. Jordi, C. J. Cotter, and S. J. Sherwin, "An adaptive selective frequency damping method," *Physics of Fluids*, vol. 27, no. 9, p. 094104, Sep. 2015, publisher: American Institute of Physics. [Online]. Available: https://doi.org/10.1063/1.4932107

[45] G. Cunha, P.-Y. Passaggia, and M. Lazareff, "Optimization of the selective frequency damping parameters using model reduction," *Physics of Fluids*, vol. 27, no. 9, p. 094103, Sep. 2015, publisher: American Institute of Physics. [Online]. Available: https://doi.org/10.1063/1.4930925

[46] B. Srinivasan and R. Rengaswamy, "Automatic oscillation detection and characterization in closed-loop systems," *Control Engineering Practice*, vol. 20, no. 8, pp. 733–746, Aug. 2012. [Online]. Available: https://doi.org/10.1016/j.conengprac.2012.02.008

[47] D. Barkley, "Linear analysis of the cylinder wake mean flow," *Europhysics Letters*, vol. 75, no. 5, pp. 750–756, Sep. 2006, number: 5 Publisher: EDP Sciences. [Online]. Available: https://doi.org/10.1209/epl/i2006-10168-7

[48] F. Guiho, F. Alizard, and J.-C. Robinet, "Global stability Analysis with Compressible CFD Solver," in *43rd Fluid Dynamics Conference*, ser. Fluid Dynamics and Co-located Conferences. American Institute of Aeronautics and Astronautics, Jun. 2013. [Online]. Available: https://doi.org/10.2514/6.2013-2620

[49] A. Pigeon, A. Levesque, and E. Laurendeau, "Two-dimensional Navier-Stokes flow solver developments at Ecole Polytechnique de Montreal," in *CFD Society of Canada 22nd Annual Conference, CFDSC*. CFD Soc. of Canada (CFDSC), 2014.

[50] A. Jameson, W. Schmidt, and E. Turkel, "Numerical solution of the Euler equations by finite volume methods using Runge Kutta time stepping schemes," in *14th Fluid and Plasma Dynamics Conference*, Palo Alto, CA, U.S.A., 1981. [Online]. Available: https://doi.org/10.2514/6.1981-1259

[51] R. Swanson and E. Turkel, "Multistage Schemes With Multigrid for Euler and Navier-Stokes Equations," NASA Langley Research Center, Technical Report 3631, 1997. [Online]. Available: https://ntrs.nasa.gov/archive/nasa/casi.ntrs.nasa.gov/19970028360.pdf

[52] B. Baldwin and H. Lomax, "Thin-layer approximation and algebraic model for separated turbulentflows," in *16th Aerospace Sciences Meeting*, ser. Aerospace Sciences Meetings. American Institute of Aeronautics and Astronautics, Jan. 1978. [Online]. Available: https://doi.org/10.2514/6.1978-257

[53] P. Spalart, "Trends in turbulence treatments," in *Fluids 2000 Conference and Exhibit*. Denver, CO, U.S.A.: American Institute of Aeronautics and Astronautics, Jun. 2000. [Online]. Available: https://doi.org/10.2514/6.2000-2306

[54] J. R. Edwards and S. Chandra, "Comparison of eddy viscosity-transport turbulence models for three-dimensional, shock-separated flowfields," *AIAA Journal*, vol. 34, no. 4, pp. 756–763, 1996. [Online]. Available: https://doi.org/10.2514/3.13137

[55] F. R. Menter, "Two-equation eddy-viscosity turbulence models for engineering applications," *AIAA Journal*, vol. 32, no. 8, pp. 1598–1605, 1994. [Online]. Available: https://doi.org/10.2514/3.12149

[56] F. R. Menter, R. B. Langtry, S. R. Likki, Y. B. Suzen, P. G. Huang, and S. Volker, "A Correlation-Based Transition Model Using Local Variables—Part I: Model Formulation," *Journal of Turbomachinery*, vol. 128, no. 3, pp. 413–422, Mar. 2004. [Online]. Available: https://doi.org/10.1115/1.2184352

[57] M. Parenteau, S. Bourgault-Cote, F. Plante, E. Kayraklioglu, and E. Laurendeau, "Development of Parallel CFD Applications with the Chapel Programming Language," in *AIAA Scitech 2021 Forum*. American Institute of Aeronautics and Astronautics, Jan. 2021. [Online]. Available: https://doi.org/10.2514/6.2021-0749

[58] P. L. Roe, "Approximate Riemann solvers, parameter vectors, and difference schemes," *Journal of Computational Physics*, vol. 43, no. 2, pp. 357–372, Oct. 1981. [Online]. Available: https://doi.org/10.1016/0021-9991(81)90128-5

[59] V. Theofilis, "Global Linear Instability," *Annual Review of Fluid Mechanics*, vol. 43, no. 1, pp. 319–352, Jan. 2011. [Online]. Available: https://doi.org/10.1146/annurev-fluid-122109-160705

[60] F. Plante and E. Laurendeau, "Simulation of Transonic Buffet Using a Time-Spectral Method," *AIAA Journal*, vol. 57, no. 3, pp. 1275–1287, 2019. [Online]. Available: https://doi.org/10.2514/1.J057224

[61] C. Rumsey, "2D Multielement Airfoil Verification - Intro Page," Jan. 2021. [Online]. Available: https://turbmodels.larc.nasa.gov/multielementverif.html

[62] T. R. Michal, J. Krakos, D. S. Kamenetskiy, M. Galbraith, C.-I. Ursachi, M. A. Park, W. K. Anderson, F. Alauzet, and A. Loseille, "Comparing Unstructured Adaptive Mesh Solutions for the High Lift Common Research Model Airfoil," in *AIAA AVIATION 2020 FORUM*. American Institute of Aeronautics and Astronautics, Jun. 2020. [Online]. Available: https://doi.org/10.2514/6.2020-3219